D1.3 WP1 Research Report II

Project Name: Anticipatory Networking Techniques in 5G and Beyond
Acronym: ACT5G
Project no.: 643002

Start date of project: 01/05/2015 **Duration:** 48 Months

This project has received funding from the European Union's Horizon 2020 research and innovation programme under the Marie Skłodowska-Curie Actions.

Document Properties

Document ID	EU-H2020-MSCA-ITN-2014-643002-ACT5G-D1.3
Document Title	D1.3 WP1 Research Report II
Contractual date of delivery to REA	Month 42
Lead Beneficiary	Linköpings universitet (LiU)
Editor(s)	D. Yuan – LiU
Work Package No.	1
Work Package Title	Network Anticipation
Nature	Report
Number of Pages	8
Dissemination Level	**PUBLIC**
Contributors	LiU: V. Angelakis, D. Yuan POLIMI: A. Capone, M. Cesana Bell labs: I. Malanchini
Version Number	1

Contents

0 Executive Summary

This is the second research report within work package one Network Anticipation of the ACT5G project. The document provides information of the conducted and expected work of early-stage researcher (ESR) one and two. The document first gives an overview of the focus area and research topics. Technical details of the work are then presented by means of research paper published or submitted since the previous research report.

1 Work Plan and Progress of ESR 1

The ESR I, Claudia Parera Sotolongo joined the project in May 1st, 2017. Her research activities include the application and development of analytics tools to real data coming from mobile radio networks, more specifically data coming from network counters, probes and drive tests. By extracting knowledge from the aforementioned data sources, the final goal is to anticipate and optimize the mobile radio network behaviour.

The main research direction includes the application of machine learning, more specifically deep and transfer learning to a wide variety of problems across the different layers of the network. During the period of May 2017 till August 2018, the ESR I has been working in a problem related to antenna tilt optimization on a real dataset from LTE stations. This work led to one conference paper and one article submitted pending of evaluation. The conference paper Transferring knowledge for tilt-dependant radio map prediction was presented in WCNC, 2018 last April. A finalized version of this work Transfer knowledge for tilt-dependant radio map prediction was submitted as journal article to the JSAC special issue on Artificial Intelligence and Machine Learning for Networking and Communications and it is under revision. During this period the ESR had the opportunity of mastering her skills on topics related to deep and transfer learning.

From September 2018 the ESR I has been working on a new domain with data related to the deployment and testing of Virtual Network Functions. This dataset is generated by the Nokia proprietary stack. Due to the complexity of the software that generates this data, first steps have include getting some preliminary insight into the data as well as the testbed architecture to evaluate the possibility of applying transfer learning to this scenario. Current open questions include evaluating the correlation between KPIs from network and orchestration domains as well as cross domain.

2 Work Plan and Progress of ESR 2

ESR2, Cristian Tatino, has focused his research on several performance aspects of millimeter-wave (mm-wave) communications. First, he has investigated the contributions to the coverage probability given by reflected paths. These, in according to the result, can represent feasible alternative paths to the direct one when this is blocked. However, reflections are generated usually by obstacle that are not the direct control of the telecom operators. Thus, ESR2 has investigated other solutions to avoid communication interruptions.

A first solution is represented by the multi-connectivity (MC). By using MC technology, a UE is able to connect with several millimeter-wave access points (mmAPs) simultaneously. In this scenarios, ESR2 has coped with the link scheduling problem for a low frequency assisted mm-wave wireless network, where a UE establishes simultaneously connections with a 5G low frequency base station (5G LB) and possibly several mmAPs. Although, multiple transmissions increase the communications reliability, at the same time they consume resources in terms of frequency band, energy, and antennas. For this reason, in this work, it is considered the possibility for a mmAP to be prepared for the communication with a UE, but without transmitting. A mmAP can be prepared for the transmission at several levels that correspond to several link states, depending on weather the mmAP is transmitting, prepared and not connected. The goal of the link scheduler (network controller, NC) is to set the state of several links along a certain time window in order to maximize the network throughput. Moreover, the mmAPs can establish a limited amount of connections because of a power budget constraint that mainly limits the number of simultaneous connections. First, the problem is formulated as non-linear binary integer optimization problem, then, it is linearized and solved by using a proposed algorithm that is based on a column generation approach. From the results it is possible to observe that the proposed solution for MC results in significant improvement of the network throughput with respect to the single connectivity case. The work has resulted in a conference paper, accepted for presentation and publication by the Resource Allocation, Cooperation and Competition in Wireless Networks (RAWNET) workshop of the 16th International Symposium on Modeling and Optimization in Mobile, Ad Hoc, and Wireless Networks (WiOPT) that will take place in May, 2018.

Moreover, Cristian Tatino has considered a further solution for increasing the reliability in mm-waves; this is the relaying technique that provides an alternative path to the direct one by using an intermediate node. More precisely, by us-

ing the knowledge acquired in queuing theory, ESR2 has analyzed the delay and the throughput for a relay-assisted mm-wave wireless network. In this work Cristian Tatino has analyzed the impact of narrow beams and directional transmissions on relaying techniques. Moreover, two transmissions schemes have been analyzed: fully directional and broadcast. By using the former, the UEs send either a packet to the destination or the relay by using narrow beams. Whereas, by using the broadcast transmission, UEs use wider beams, with lower beamforming gain, in order to send a packet to both the mmAP and the relay in the same timeslot. At first, ESR2 has analyzed the performance of the queue at the relay and then the throughput and the delay. The result has shown when it is beneficial to use either narrow beams (fully directional) or wider beams (broadcast). Furthermore, the numerical evaluation of the analytical analysis and the simulations have shown the impact of the beamfoming alignment on the network performance. This investigation has resulted to a submitted journal paper and in a conference paper, accepted for presentation and publication by the Emerging Technologies for 5G and Beyond Wireless and Mobile Network (ET5GB) workshop of the IEEE Global Communications Conference (Globecom) that will take place in December, 2018.

As next steps, Cristian Tatino is 1) considering link scheduling problems for multi-connectivity with non-perfect prediction, and 2) analyzing the network performance of relay-assisted mm-wave wireless networks for several non-random transmission policies.

3 Appendices:

- Transferring knowledge for tilt-dependant radio map prediction (published in IEEE WCNC, 2018)
- Transfer knowledge for tilt-dependant radio map prediction (under revision of the IEEE JSAC special issue on Artificial Intelligence and Machine Learning for Networking and Communications, 2018)
- Maximum throughput scheduling for multi-connectivity in millimeter-wave networks (published in WiOPT Workshops, 2018)
- Throughput analysis for relay-assisted millimeter-wave wireless networks (accepted by IEEE Globecom Workshops, 2018)

Transferring Knowledge for Tilt-Dependent Radio Map Prediction

Claudia Parera*, Alessandro E. C. Redondi*, Matteo Cesana*, Qi Liao†, Lutz Ewe† and Cristian Tatino‡
*DEIB, Politecnico di Milano, Milan, Italy
†Nokia Bell Labs, Stuttgart, Germany
‡Linköping University, Linköping, Sweden
E-Mails: {claudia.parera, alessandroenrico.redondi, matteo.cesana}@polimi.it
{qi.liao, lutz.ewe}@nokia-bell-labs.com, cristian.tatino@liu.se

***Abstract*—Fifth generation wireless networks (5G) will face key challenges caused by diverse patterns of traffic demands and massive deployment of heterogeneous access points. In order to handle this complexity, machine learning techniques are expected to play a major role. However, due to the large space of parameters related to network optimization, collecting data to train models for all possible network configurations can be prohibitive. In this paper, we analyze the possibility of performing a knowledge transfer, in which a machine learning model trained on a particular network configuration is used to predict a quantity of interest in a new, unknown setting. We focus on the tilt-dependent received signal strength maps as quantities of interest and we analyze two cases where the knowledge acquired for a particular antenna tilt setting is transferred to (i) a different tilt configuration of the same antenna or (ii) a different antenna with the same tilt configuration. Promising results supporting knowledge transfer are obtained through extensive experiments conducted using different machine learning models on a real dataset.**

***Index Terms*—Radio map prediction, antenna tilt, machine learning, knowledge transfer**

I. Introduction

The fifth generation wireless networks (5G) are expected to support a series of unique features compared to current architectures, including more users, higher data rates, reduced latency and improved energy efficiency. To reach these goals, 5G will leverage the availability of dense and heterogeneous deployments coupled with novel technologies able to be dynamically managed both in a centralized or distributed manner. To cope with such a complex scenario, it is envisioned that machine learning tools will play a major role in enabling the transition from current mobile networks to the future 5G architecture [1]. By exploiting the constantly increasing availability of data from both network devices and user terminals, such tools will assist network operators in facing the increasing complexity in the setting of the control parameters for network optimization, forming the basis for automatic and smart network management techniques.

Among the many parameters that can be configured at the base station (BS), one of the most important is the antenna tilt, that is the angle formed by the vertical direction of the antenna with the horizon. Antenna tilt can be realized either mechanically (by physically inclining the antenna up or down) or electrically (relying on beamforming techniques that steer the main beam of the antenna towards a desired vertical direction), or even as a combination of the two. The antenna tilt directly impacts on many performance measures of the cell served by a BS, such as coverage, signal strength, and inter-cell interference, which in turn determine the quality of service experienced by the end users.

From an operator perspective, being able to predict such performance measures without performing extensive trials or measurement campaigns is of key importance for at least two reasons: first, extensive measurement campaigns such as test driving are time consuming and costly. Secondly, even assuming that measurements can be obtained in a cheap way (e.g., directly from user terminals through crowdsourcing), this requires that all possible antenna tilts are tested, which can easily cause issues on the cell performance and decrease the perceived quality of service. Therefore, such tests could be realistically performed only for very short periods and during off-peak traffic hours, making the idea of obtaining data measurements from users unfeasible.

Given such difficulties, an option which may be particularly appealing to network operators is to transfer the knowledge acquired through a single measurement campaign (e.g., for a given antenna tilt setting) to a new domain (e.g., a new tilt setting) without needing to acquire a complete set of additional measurements. Such a learning paradigm, in which the data distributions of the training (source) and testing (target) sets are significantly different, can be seen as an example of *transfer learning* and has received increasing attention in the last few years [2].

In this paper, we study the possibility of performing such a knowledge transfer for the task of predicting the radio signal strength map of a particular BS cell. We start from a dataset of signal strength measurements obtained from real-life long term evolution (LTE) base stations and analyze the performance of several machine learning algorithms in two different scenarios where the knowledge acquired for a particular antenna tilt setting is transferred to (i) a different tilt configuration of the same antenna or (ii) a different antenna with the same tilt

This work is funded by the European Union's Horizon 2020 research and innovation programme under the Marie Sklodowska-Curie grant agreement No. 643002.

configuration.

We show through extensive experiments that transferring knowledge allows for promising prediction performance and that the domain similarity (the difference between training and testing data distributions) plays a role in selecting the machine learning technique that obtains the best performance.

The rest of this paper is organized as it follows: Section II reviews related works in the area of network planning and optimization, with particular focus on those works dealing with antenna tilt. Section III describes in details the scenario under consideration, while Section IV focuses on the machine learning tools used for this work. Experiments and discussion on the obtained results are reported in Section V. Finally, Section VI concludes the paper and describes future work directions.

II. Related Work

Recent works have studied the importance of antenna tilt in the context of network planning and optimization problems.

The literature can be broadly categorized in two areas: (i) network optimization through antenna tilt adjustment and (ii) prediction of tilt-dependent radio maps. With reference to the former area, in [3], a method for finding the optimal antenna tilts in a heterogeneous network is proposed. The method is built on a reinforcement learning algorithm which adapts the antenna tilts to the specific network load conditions in order to maximize the user throughput fairness and the overall energy efficiency. Results on simulated data demonstrate that the proposed method outperforms a fixed strategy for the antenna tilts. A similar approach is taken by the authors of [4], where reinforcement learning is again used to optimize the antenna tilts, this time with the objective of maximizing the overall data rate of the network. Finally, the work in [5] proposes a general machine learning-based network planning tool. The flexibility of the approach is demonstrated with examples, including readjusting the antenna tilts to compensate for loss of service caused by faulty cells.

As for the second area of works, the work in [6] proposes a geometrical-based extension to different traditional log-distance path loss models (Okumura-Hata, Walfisch-Ikegami) to take into account the antenna tilt during the prediction of the signal strength at a given distance from the base station. The proposed extension, named vertical gain correction (VGC), is calculated directly from the antenna patterns provided by the manufacturer and is added to the signal strength estimated by the path loss models to compensate for the antenna tilt. Experimental results on data collected from LTE base stations show that the VGC improves the signal strength prediction performance compared to traditional models. Such method is then used to compute predictions that are used in a following work [7] to optimize the antenna tilts in order to maximize the capacity and coverage of a simulated LTE network. The predictive performance are reported to be lower for locations close to the antenna. Similarly, the work in [8] investigates the effect of antenna tilt on radio maps, comparing the path loss models developed by 3GPP for different propagation environments [9] with the results obtained by a ray tracing tool able to take into account antenna tilts. Results demonstrate that changing antenna tilt has a significant impact on the shadowing map, therefore calling for a rethinking of currently available 3GPP propagation models and assumptions, which apply identical shadowing map independently from the antenna tilt.

Our work shares the same research objectives of this second class with one fundamental novelty: in all the aforementioned works, the domain of the data used for predicting the signal strength is similar (if not the same) to the target domain; as an example, the signal strength radio map of an antenna under a given tilting configuration is interpolated or predicted out of available signal strength samples collected for the same antenna in the same tilting configuration. We also analyze the cases where the performance of target antenna configuration is predicted by using training dataset collected under different configurations or even referring to a totally different antenna.

III. Problem Statement and Background

In this paper we address the following problem in mobile radio networks: *"how to predict the performance of a given network configuration by leveraging performance information of diverse network configurations"*. The performance measure that we target here is the received signal strength in the downlink and the network configuration domains include the tilting configuration of the emitting base stations.

Assume K base stations are deployed in the area under analysis. Each base station can work in H different tilt configurations, indexed by $h = 1, \ldots, H$. Let $s_{k,h}(\mathbf{x}_i)$, be the measured signal strength received at location $\mathbf{x}_i = \{y_i, z_i\}$, from the k-th base station when running the h-th tilt configuration, where y_i and z_i indicate the latitude and the longitude of the i-th location, respectively. Let $\mathcal{M}_k^h$ be the set of location indexes where measurements for base station k running configuration h have been taken.

The problem at hand can be defined as follows: given $\left\{s_{k,h}(\mathbf{x}_i) : i \in \mathcal{M}_k^h\right\}$, estimate the unknown signal strength $\hat{s}_{m,n}(\mathbf{x}_j)$ at the same or different locations, $\mathbf{x}_j$, under diverse and different network configuration domains, that is $\mathbf{x}_j$, $j \in \mathcal{M}_m^n$ with $m \neq k$ and/or $n \neq h$.

The dataset used in this work is composed of reference signal received power (RSRP) outdoor measurements collected in Espoo, Finland in November 2016 out of two LTE commercial base stations with three different 120° sectors each and operating at 2.6 GHz (see Fig. 1 reporting the positions of the two antennas and the representation of the target area). Out of the two antennas, we focus here on three physical cell identifiers (PCIs) which will be referred to as PCI 1, 2 and 3. PCIs 1 and 2 refer to two different sectors of the same base stations, whereas PCI 3 is a sector of a totally different base station.

The RSRP measurements were collected using an Android device equipped with an application capable of storing the RSRP from all the received cells, the cell identifier, the GPS position of the device and the timestamp. Such measurements were carried out at a frequency of 1 Hz while walking along

PCI	total tilt setting (in degrees)
1	3,5,6,7,9
2	3,5,6,7,9
3	5,6,9

TABLE I: Available down-tilt configurations.

Fig. 1: Map showing the base stations position and the PCIs (sectors) in the reference dataset.

a route of about 8 km within each cell coverage area, with a minimum and maximum distance from the base station of 30 m and 900 m respectively. The testing paths were designed to include varied propagation conditions: university campus with two- or three-story buildings, residential areas, parking lots, lower density rural and open area with different types of roads (i.e. pedestrian, cycling and main roads). Each testing path was walked once for each electronic tilt setting. The different tilt configurations are shown in Table I. The receiver was placed at the height of 1.5 m and always kept with the same orientation. The weather conditions were stable and cloudy and the road was covered by snow for most of the measurement campaign. In total, about $3 \cdot 10^5$ RSRP measurements were obtained. Each observation contains the following fields: the measurement position, the RSRP value, the corresponding PCI and the timestamp. The raw dataset was pre-processed to remove outliers and corrupted samples: as an example, at the beginning of each experiment the GPS receiver takes some time to set up, recording incorrect position. Moreover, the RSRP values are averaged over grid segmentation of the map, with the grid size of 20 m $\times$ 20 m. After the pre-processing steps, the dataset was reduced to about $3.5 \cdot 10^3$ observations per PCI and per tilt configuration, for a total of about $5 \cdot 10^4$ measurements.

IV. Prediction Approaches

In this section, we describe two different prediction approaches. The first one leverages spatial information only (latitude and longitude) to predict the signal strength; conversely, the second approach adopts a larger set of features to capture path loss and propagation properties.

A. Location-Only Approaches

Based on the strong spatial correlation between signal strength and location, three different techniques have been used:

Baseline: The *Baseline (B)* method takes as the predicted value of signal strength for a target position $\mathbf{x}$ the signal strength of the closest point $\mathbf{x}_i$ available in the training dataset $\mathcal{M}$. This method is essentially k-nearest neighbors (k-NN) with $k = 1$. Formally,

$$\hat{s}(\mathbf{x}) = s(\mathbf{x}_i), \qquad \mathbf{x}_i = \underset{\mathbf{x}_i, i \in \mathcal{M}}{\arg\min}\, d(\mathbf{x}, \mathbf{x}_i). \tag{1}$$

Adjusted Baseline: As proposed in [6], the *Baseline* method can be extended by leveraging *a priori* information on the radiation pattern of the reference antenna. Formally, the *Adjusted Baseline (AB)* predicts the value of the signal strength as:

$$\hat{s}(\mathbf{x}) = s(\mathbf{x}_i) + \Delta_H(\mathbf{x}, \mathbf{x}_i) + \Delta_V(\mathbf{x}, \mathbf{x}_i),\ \mathbf{x}_i = \underset{\mathbf{x}_i, i \in \mathcal{M}}{\arg\min}\, d(\mathbf{x}, \mathbf{x}_i), \tag{2}$$

being $\Delta_H(\mathbf{x}, \mathbf{x}_i)$ and $\Delta_V(\mathbf{x}, \mathbf{x}_i)$ the difference of the antenna horizontal and vertical gain respectively in the directions towards the target position $\mathbf{x}$ and the closest known position $\mathbf{x}_i$. Formally,

$$\Delta_H(\mathbf{x}, \mathbf{x}_i) = \eta(\mathbf{x}) - \eta(\mathbf{x}_i) \text{ and } \Delta_V(\mathbf{x}, \mathbf{x}_i) = \gamma(\mathbf{x}) - \gamma(\mathbf{x}_i),$$

where $\eta()$ and $\gamma()$ are the horizontal and vertical gain of the antenna respectively.

k-Nearest Neighbors with Inverse Distance Weighting: This technique extends the classical nearest neighbor approaches [10] and predicts the signal at an unknown target location as a weighted average of the signals at the k closest known locations:

$$\hat{s}(\mathbf{x}) = \sum_{i \in \mathcal{M}(\mathbf{x})} w_i s(\mathbf{x}_i). \tag{3}$$

The set $\mathcal{M}(\mathbf{x})$ includes the indexes of the k locations which are geographically closest to the target unknown location $\mathbf{x}$. Weights w_i are chosen to be inversely proportional to the distance $d(\mathbf{x}_i, \mathbf{x})$ and normalized to sum to unity, that is:

$$w_i = \frac{d(\mathbf{x}_i, \mathbf{x})^{-1}}{\sum_{j \in \mathcal{M}(\mathbf{x})} d(\mathbf{x}_j, \mathbf{x})^{-1}}. \tag{4}$$

B. Geometric-aware Approaches

Location-only approaches tend to produce good results under ideal conditions, when the available labeled dataset is rich enough and the reference area is sampled uniformly. On the other hand, when the available dataset is sparsely sampled in space, then the location-only approaches may fail. Therefore, we have resorted to more complex prediction models leveraging additional features besides location. Namely, being $\mathbf{x}_A$ the antenna location and $\mathbf{x}$ the target position, the following set of features is considered for the prediction task (see Figure 2):

- the physical *distance* between the antenna and the measurement position, $d(\mathbf{x}, \mathbf{x}_A)$;
- the *relative elevation angle* between the down-tilt of the antenna and the vertical direction from the antenna emitting element to the measurement position, defined as:

$$\delta_1 = 90^\circ - (\alpha_A + \alpha_E), \tag{5}$$

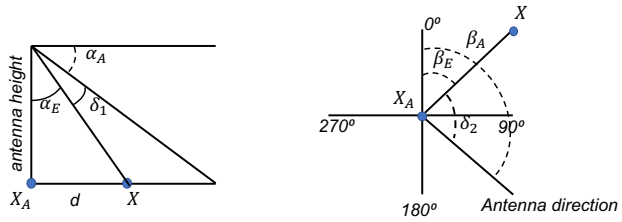

Fig. 2: Relative angles in the vertical (left) and horizontal (right) planes between the antenna pointing direction and the direction towards the test position $\mathbf{x}$.

being α_A the antenna down-tilt (mechanical plus electrical) and α_E the angle at which the antenna "sees"the target position;

- the *relative azimuth* between the horizontal orientation of the antenna and the horizontal direction to the measurement position defined as:

$$\delta_2 = \beta_A - \beta_E, \tag{6}$$

being β_A the horizontal orientation of the antenna and β_E the horizontal orientation of the target position with respect to the antenna position.

- the *tilt* configuration of the antenna, α_A.

Each signal strength sample in the training dataset is therefore associated to a feature vector $\mathcal{X} = \{1, d, \delta_1, \delta_2, \alpha_A\}^T$, after applying the logarithm transformation to d, given that RSRP samples are measured in dBm.

Multivariate Linear Regression: A linear model can be trained to relate the measured signal strength in a position to the corresponding feature vector. Given a target position $\mathbf{x}$, the predicted signal strength is modeled as:

$$\hat{s}(\mathbf{x}) = \mathbf{\Theta}^T \mathcal{X},$$

being $\mathbf{\Theta}$ the parameter vector of the linear model.

Random Forest: Random forest (RF) is one of the ensemble methods used for classification and regression purposes. The algorithm introduced by Ho [11] in 1995, and later extended by Breiman and Cutler [12], uses the idea of bagging to perform predictions. During the process several trees are grown independently using different bootstrapped samples of the data and majority voting or averaging are used for the final prediction. In contrast to traditional trees, the variable used to perform the split in each node is chosen randomly from a set of predictors [12]. RF is known to sometimes outperform other machine learning techniques such as Neural Networks due to its resistance to overfitting [13].

XGBoost: Boosting is a technique that can be used to improve the performance of a generic machine learning algorithm, by iteratively tuning a model each time giving more importance to mispredicted test samples [14]. Here we use a particular version of boosting called XGBoost [15], which unifies several ideas: Gradient Boosting, regularization to avoid over fitting, column sampling taken from RF and sparse data manipulation.

V. Experiments

Inspired by the concept of *transfer learning* [2], we evaluate here the performance of different prediction approaches when varying the *degree of similarity* of the datasets (domains) used for training and testing. The quantitative measure to capture domain similarity used in the analysis is the Kullback-Leibler divergence index (KL) [16] which measures the relative entropy of a given probability distribution with respect to another one. Namely, given two reference datasets, one used for training and one used for testing, we derive the KL divergence indexes of the probability distributions of the logarithm of the distance (d), relative angle (δ_1) and relative azimuth (δ_2) of the two datasets. In details, the range of distances, relative angles and relative azimuth contained in the two datasets was uniformly quantized to k intervals, further deriving the related discrete probability distributions. For example, the symmetric KL divergence index of the distance probability distributions in one training and one testing dataset is given by:

$$D_{KL}(d) = \sum_{i=1}^{k} P_d^{(\text{tr})}(i) \log \frac{P_d^{(\text{tr})}(i)}{P_d^{(\text{te})}(i)} + \sum_{i=1}^{k} P_d^{(\text{te})}(i) \log \frac{P_d^{(\text{te})}(i)}{P_d^{(\text{tr})}(i)}, \tag{7}$$

where $P_d^{(\text{tr})}(i)$ and $P_d^{(\text{te})}(i)$ with $i = 1 \dots k$ defining the discrete probability distributions of the distance in the training and testing dataset respectively. Similar definitions hold for the KL divergence indexes related to the relative angle, δ_1 and relative azimuth δ_2. Finally, to give a more succinct representation of domain similarity, we introduce the domain distance measure (DD) by summing the three indexes together, that is:

$$\text{DD} = D_{KL}(d) + D_{KL}(\delta_1) + D_{KL}(\delta_2). \tag{8}$$

Prediction quality is assessed through the mean absolute error (MAE) and the mean absolute percentage error (MAPE), defined in Eq. (9), Eq. (10), respectively, where n is the number of target positions in the testing dataset.

$$\text{MAE}(s, \hat{s}) = \frac{1}{n} \sum_{i=0}^{n-1} |s_i - \hat{s}_i| \tag{9}$$

$$\text{MAPE} = \frac{100}{n} \sum_{i=0}^{n-1} \left| \frac{s_i - \hat{s}_i}{s_i} \right|. \tag{10}$$

A. Tilt-to-Tilt Knowledge Transfer

In *Tilt-to-Tilt* knowledge transfer, we use a dataset obtained under a given tilt setting to predict the performance of the same antenna under a different tilt configuration. Table II reports the results obtained by the different prediction approaches described in Section IV when considering PCI 1 and different combinations for the training and testing tilt conditions. The text in the table header explains the knowledge transfer involved in the experiment: as an example, the first two columns (2→3) refer to the case where the training set was obtained with an antenna tilt of 2 degrees and the tilt configuration for the test set was 3 degrees.

	Tilt 2 ->Tilt 3		Tilt 4 ->Tilt 3		Tilt 6 ->Tilt 3	
	DD 0.21		DD 0.55		DD 2.58	
	MAE	MAPE%	MAE	MAPE%	MAE	MAPE%
B	4.02	4.03	5.27	5.23	7.15	7.31
AB	4.45	4.47	7.49	7.64	11.03	10.86
k-NN	3.9	3.92	5.26	5.19	6.69	6.83
LR	7.75	8.2	7.6	8.1	8.15	8.83
RF	3.89	4.11	5.41	5.38	6.06	6.02
XGB	4.33	4.41	4.68	4.89	6.25	6.59

TABLE II: Prediction performance of different algorithms under *tilt-to-tilt* knowledge transfer for reference PCI 1.

From the results in Table II, we can make the following observations.

- The prediction error is impacted by the training and test domain distance. As the domain distance increases, the prediction performance decreases for all tested algorithms.
- Notably, location-only approaches (first three rows in Table II) and geometric-aware prediction approaches (last three rows) perform similarly when domain distance is small, whereas geometric-aware approaches have better performance when the domain distance increases. This is because, geometric-aware approaches better capture the physical properties of channel propagation, thus being more robust against the cross-domain missing information.
- RF generally provides a good prediction performance, regardless of the domain difference.

Similar results obtained for other PCIs are not reported here for the sake of brevity.

To further investigate the impact of the domain distance measure, we have considered the cases where the training dataset is integrated with samples taken from the test domain. Figure 3 refers to the cases where increasing percentages of the training dataset samples (tilt configuration 6) are replaced by samples from the testing domain (tilt configuration 3). Sampling is performed randomly and results are averaged over 10 different trials. Fig. 3a and Fig. 3b report the value of the Domain Distance measure and the MAPE when varying the percentage of testing samples added to the training datasets. All tested methods show decreasing prediction error as the distance between domains decreases.

B. PCI-to-PCI Knowledge Transfer

In case of PCI-to-PCI knowledge transfer, a dataset referring to one antenna and a given tilt configuration is used to train the models to predict the signal strength of another antenna in the same tilt configuration. Table III reports the same information as Table II when training and test datasets refer to different antennas (PCIs). In general, the prediction error is higher with respect to the case of *Tilt-to-Tilt* knowledge transfer as training and test datasets are more dissimilar. As already observed in case of *Tilt-to-Tilt* knowledge transfer, the error is smaller when the domain difference is smaller for all the tested algorithms.

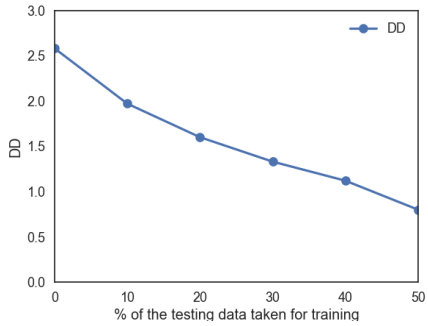

(a) Domain Distance (DD)

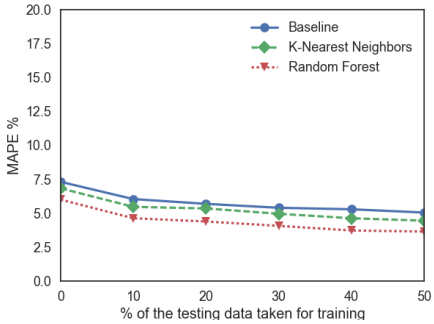

(b) MAPE

Fig. 3: Relationship between Domain Distance and MAPE (a), (b): training on tilt 6, testing on tilt 3 for PCI 1.

	PCI 1 ->PCI 2		PCI 3 ->PCI 2	
	DD 1.89		DD 1.76	
	MAE	MAPE%	MAE	MAPE%
B	8.41	8.63	10.27	11.09
AB	8.41	8.63	10.27	11.09
k-NN	8.2	8.43	10.27	11.08
LR	11.39	11.21	8.53	8.95
RF	11.37	11.2	8.58	8.85
XGB	11.06	10.97	8.88	9.02

TABLE III: Prediction performance of different algorithms under *PCI-to-PCI* knowledge transfer for reference tilt 2.

The same strategy of taking samples of the testing data to train the model can be applied when transferring knowledge from PCI to PCI. Figures 4a and 4b report the value of the Domain Distance measure and the average prediction error when varying the percentage of samples from the testing domain (PCI 2) added to the training datasets (PCI 1). Figures 4c and 4d report the same graphs for the case of training over PCI 3 and testing over PCI 2. In both cases the average error decreases sharply when adding 20% of the testing dataset to the training dataset. Notably, the prediction performance levels off and does not improve much when going beyond 20%.

VI. Conclusions

In this paper we addressed the problem of predicting the signal strength in the downlink of a real LTE network where the antennas can be tuned to operate with different tilting antenna configurations. Different prediction approaches

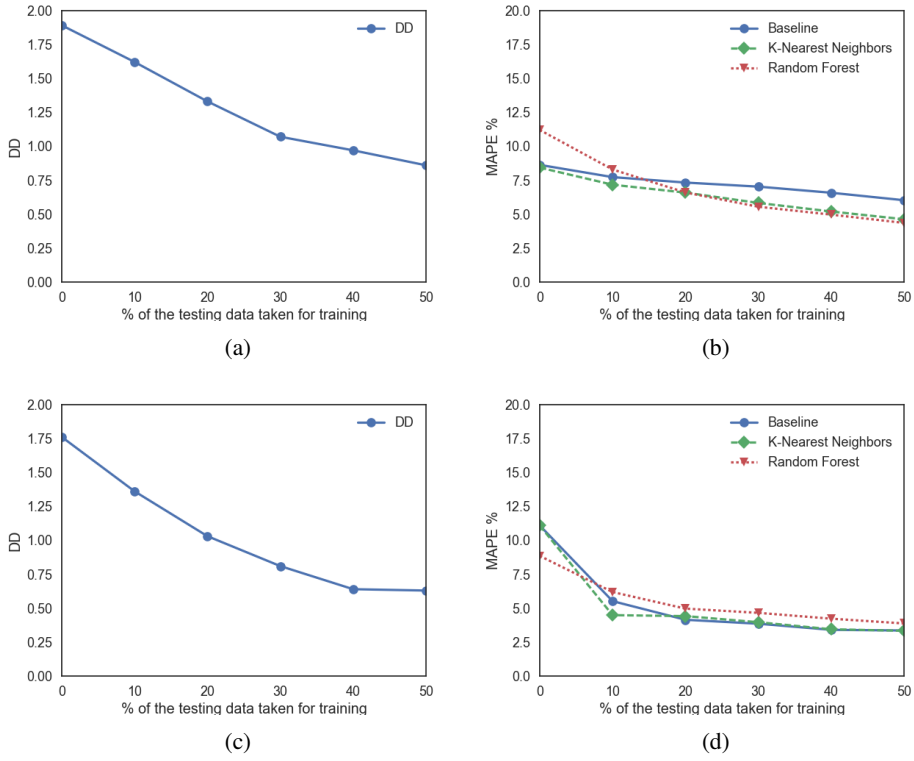

Fig. 4: DD vs MAPE. (a),(b): training on PCI 1, testing on PCI 2. (c),(d): training on PCI 3, testing on PCI 2 at tilt 2.

were considered with increasing complexity, starting from models/approaches only leveraging location information to predict the signal strength up to models/approaches based on more refined features related to propagation and antenna configuration. As opposed to other works in the field of radio map inference, we studied the quality of prediction of the aforementioned approaches when the datasets used for training and testing have different statistical characteristics. We observed that the performance of the predictive models is highly dependent on the difference between data distributions of the training and testing domain. Thus, analyzing domain similarity plays a crucial role in selecting the best performing model. Furthermore, two approaches are applied to further reduce the domain difference: (i) choosing the training set obtained from a tilt setting with higher similarity to the testing domain, and (ii) adding to the training set a limited number of samples from the testing domain. Future work will analyze possible strategies to achieve good tradeoff between improving prediction performance and reducing measuring effort for cross-domain data collection.

References

[1] C. Jiang, H. Zhang, Y. Ren, Z. Han, K.-C. Chen, and L. Hanzo, "Machine learning paradigms for next-generation wireless networks," *IEEE Wireless Communications*, vol. 24, no. 2, pp. 98–105, 2017.

[2] S. J. Pan and Q. Yang, "A survey on transfer learning," *IEEE Transactions on knowledge and data engineering*, vol. 22, no. 10, pp. 1345–1359, 2010.

[3] W. Guo, S. Wang, Y. Wu, J. Rigelsford, X. Chu, and T. O'Farrell, "Spectral-and energy-efficient antenna tilting in a hetnet using reinforcement learning," in *Wireless Communications and Networking Conference (WCNC), 2013 IEEE*. IEEE, 2013, pp. 767–772.

[4] N. Dandanov, H. Al-Shatri, A. Klein, and V. Poulkov, "Dynamic self-optimization of the antenna tilt for best trade-off between coverage and capacity in mobile networks," *Wireless Personal Communications*, vol. 92, no. 1, pp. 251–278, 2017.

[5] J. Moysen, L. Giupponi, and J. Mangues-Bafalluy, "A mobile network planning tool based on data analytics," *Mobile Information Systems*, vol. 2017, 2017.

[6] I. Rodriguez, H. C. Nguyen, T. B. Sørensen, J. Elling, M. B. Gentsch, M. Sørensen, L. Kuru, and P. Mogensen, "A geometrical-based vertical gain correction for signal strength prediction of downtilted base station antennas in urban areas," in *Vehicular Technology Conference (VTC Fall), 2012 IEEE*. IEEE, 2012, pp. 1–5.

[7] H. C. Nguyen, I. Rodriguez, T. B. Sorensen, J. Elling, M. B. Gentsch, M. Sorensen, and P. Mogensen, "Validation of tilt gain under realistic path loss model and network scenario," in *Vehicular Technology Conference (VTC Fall), 2013 IEEE 78th*. IEEE, 2013, pp. 1–5.

[8] D. W. Kifle, B. Wegmann, I. Viering, and A. Klein, "Impact of antenna tilting on propagation shadowing model," in *Vehicular Technology Conference (VTC Spring), 2013 IEEE 77th*. IEEE, 2013, pp. 1–5.

[9] 3GPP, "Evolved universal terrestrial radio access (e-utra); further advancements for (e-utra) physical layer aspects," *TR 36.814, Techincal report*, 2006.

[10] T. Cover and P. Hart, "Nearest neighbor pattern classification," *IEEE transactions on information theory*, vol. 13, no. 1, pp. 21–27, 1967.

[11] T. K. Ho, "Random decision forests," in *Document Analysis and Recognition, 1995., Proceedings of the Third International Conference on*, vol. 1. IEEE, 1995, pp. 278–282.

[12] A. Liaw, M. Wiener *et al.*, "Classification and regression by randomforest," *R news*, vol. 2, no. 3, pp. 18–22, 2002.

[13] L. Breiman, "Random forests," *Machine learning*, vol. 45, no. 1, pp. 5–32, 2001.

[14] ——, "Arcing the edge," Technical Report 486, Statistics Department, University of California at Berkeley, Tech. Rep., 1997.

[15] T. Chen and C. Guestrin, "Xgboost: A scalable tree boosting system," in *Proceedings of the 22nd acm sigkdd international conference on knowledge discovery and data mining*. ACM, 2016, pp. 785–794.

[16] J. M. Joyce, "Kullback-leibler divergence," in *International Encyclopedia of Statistical Science*. Springer, 2011, pp. 720–722.

Transfer Learning for Tilt-Dependent Radio Map Prediction

Claudia Parera*†, Alessandro E. C. Redondi*, Matteo Cesana*, Qi Liao†, Ilaria Malanchini† and Cristian Tatino‡†

Abstract

Machine learning will play a major role in handling the complexity of fifth generation wireless networks by supporting and augmenting network management and orchestration capabilities. However, due to the large amount of parameters that can be used for network optimization, collecting labeled data to train models for all possible network configurations can be prohibitive. In this work, we explore the applicability of transfer learning techniques for radio map prediction. Namely, we analyze the case in which the knowledge acquired for a given antenna tilt setting is transferred to a different tilt configuration of the same antenna in order to predict the signal strength map of the new, unknown setting. We test our algorithm in two different scenarios: (i) where training data is obtained from real measurements, and (ii) where training data is artificially generated. In both cases we evaluate the performance against standard benchmark machine learning techniques. The experimental results show that the proposed transfer learning approach achieves notable prediction accuracy with a mean absolute percentage error below 5%. Furthermore, when lacking real measurements, our approach still achieves comparable performance by substituting almost 80% of the training samples with artificially generated data.

Index Terms

Radio map prediction, antenna tilt, transfer learning, artificial data generation.

*DEIB, Politecnico di Milano, Milan, Italy. †Nokia Bell Labs, Stuttgart, Germany. ‡Linköping University, Linköping, Sweden.

This work is funded by the European Union's Horizon 2020 research and innovation programme under the Marie Sklodowska-Curie grant agreement No. 643002.

This work extends the preliminary study in [1].

I. Introduction

Fifth generation wireless networks (5G) are expected to enhance a series of features present in current architectures. Such enhancements include: more users, higher data rates, reduced latency and improved energy efficiency. To achieve this, 5G leverages the availability of dense and heterogeneous deployments coupled with novel technologies, which can be dynamically managed in either a centralized or distributed manner. To cope with such a complex scenario, it is envisaged that machine learning tools will play a major role in enabling the transition from current mobile networks to future 5G architectures [2]. Data from both network devices and user terminals is increasing in availability. By exploiting this, machine learning tools will be able to assist network operators in dealing with the increasing complexity of configuring parameters for network optimization; thus, forming the basis for automatic and smart network management techniques.

Among the manifold parameters that can be configured at the base station (BS), one of the most important is the antenna tilt, which is the angle formed by the vertical direction in which the antenna is facing and the horizon. Antenna tilt can be controlled either mechanically (by physically inclining the antenna up or down) or electronically (relying on beamforming techniques that steer the main beam of the antenna towards a desired vertical direction), or even by a combination of the two. The antenna tilt directly impacts the performance measures of a cell served by a BS: network coverage, signal strength and inter-cell interference. These factors determine the quality of service experienced by the end users.

From an operator's perspective, being able to predict such performance measures without carrying out extensive trials or measurement campaigns is of key importance for two reasons: firstly, extensive measurement campaigns, such as test driving, are time consuming and costly. Secondly, even if we assume that measurements can be obtained inexpensively (e.g., directly from user terminals through crowd-sourcing), testing all possible antenna tilts is still required. This can easily impact cell performance and decrease the quality of service. Realistically, such tests could be performed for only very short periods of time, and during off-peak traffic hours. Obtaining data in this way is therefore infeasible.

Given such difficulties, a solution which may be particularly appealing to network operators is transferring the knowledge acquired from a single measurement campaign (for a given antenna

tilt setting) to a new *domain* (a new tilt setting) without needing to acquire a complete set of additional measurements. In this case, the data distributions of the training (source) and testing (target) sets are different. Therefore, we formalize and solve this problem via *transfer learning*, a paradigm that has received increased attention in the last few years [3].

In this paper, we study the possibility of performing transfer learning for the task of predicting the radio signal strength map of a particular BS. We start from a dataset of signal strength measurements collected from real-life, commercial, long term evolution (LTE) BSs and analyze the performance of a transfer learning approach based on a deep neural network, where a *domain* is defined as the knowledge acquired for a particular antenna tilt setting. This is then transferred to a different *domain*, i.e., a different tilt configuration of the same antenna. As benchmark, we compare the prediction performance of our proposed method against the performance of standard machine learning techniques when applied to the same problem. The performance evaluation is carried out in two different scenarios: (i) the data chosen for training is only obtained from real measurements and (ii) the training data is artificially generated.

In summary, the main contributions of this paper are as follows:

- We propose a transfer learning framework based on a deep neural network for tilt-dependent radio map prediction. We evaluate its prediction performance by comparison to standard machine learning approaches. The proposed approach is shown to achieve notable prediction accuracy and it is stable when encountering differences between the training domain and the testing domain.
- Our analysis shows that, decreasing the amount of real measurements taken from the testing domain, the prediction performance does not decrease significantly. This being the case, we propose a method to quantify the minimum amount of real measurements required during the training phase; while keeping a balance between prediction performance and the amount of labeled data required from the target domain.
- We test our approach using artificially generated data as source domain. We show that by using transfer learning and artificially generated data, we can significantly decrease the amount of labeled data required during the training phase, without affecting the prediction performance.
- We provide a method to generate data artificially at no cost for the operator.

The rest of this paper is organized as follows: Section II reviews related work in the area of

network planning and optimization, with particular focus on those works dealing with antenna tilt. It further reviews the state of the art of transfer learning, and its applications in the area of network planning and optimization. Section III describes in details the considered scenario as well as preliminary data collection and data preprocessing steps. Section IV focuses on the machine learning tools used for this work. Experiments and discussion of the obtained results, with special emphasis on the use of artificial data, are reported in Section V. Finally, Section VI concludes the paper.

II. Background and Related Work

In this section, we briefly review the works on antenna tilt-dependent radio map prediction, introduce some background information on transfer learning, and present some applications of transfer learning techniques to wireless networks.

A. Tilt-Dependent Radio Map Prediction

Tilt-dependent radio map prediction plays a crucial role in the context of network planning and proactive network optimization [4]. The predicted propagation condition can be exploited for a reliable decision making process to dynamically optimize antenna tilts in a time-varying network environment [4], [5]. Although radio map prediction has been extensively studied [6], its dependence on antenna tilt has been investigated only in few works. The authors in [7] propose a geometrical-based extension to various traditional log-distance path loss models (Okumura-Hata, Walfisch-Ikegami) to take into account the antenna tilt during the prediction of the signal strength at a given distance from the BS. The proposed extension, named vertical gain correction (VGC), is calculated directly from the antenna patterns provided by the manufacturer and is added to the signal strength estimated by the path loss models to compensate for the antenna tilt. Experimental results on data collected from LTE BSs show that the VGC improves the performance of signal strength prediction compared to traditional models. Similarly, the work in [8] investigates the effect of antenna tilt on radio maps, comparing the path loss models developed by 3rd generation partnership project (3GPP) for different propagation environments [9] with the results obtained by a ray tracing tool able to take into account antenna tilts. Results demonstrate that changing antenna tilt has a significant impact on the shadowing map, therefore calling for a rethinking

of currently available 3GPP propagation models and assumptions, which apply an identical shadowing map independently from the antenna tilt.

B. Overview of Transfer Learning

Traditional machine learning algorithms work under the assumptions that training and testing data are taken from the same distribution and have the same feature space. However, in real world applications these assumptions do not always hold. Firstly, the data distribution may not be static, but vary over time, making it difficult to apply a trained model to a new scenario at a different time period. Secondly, training and testing data could also differ in terms of geographic location, or the equipment used for recording the measurements (e.g., a different mobile device). In such cases, transfer learning is a promising approach for exploiting and sharing knowledge among different domains.

Transfer learning extracts knowledge from one or more source tasks and applies it to a target task; allowing the domains and tasks to be different. In this paper, a *domain* $\mathcal{D} := \{\mathcal{X}, P(X)\}$ consists of a feature space $\mathcal{X}$ and a marginal probability distribution $P(X)$ for $X \in \mathcal{X}$, and a *task* $\mathcal{T} := \{\mathcal{Y}, f(\cdot)\}$ consists of a label space $\mathcal{Y}$ and an objective predictive function $f(\cdot)$. From a probabilistic point of view, $f(\cdot)$ can be written as $P(Y|X)$ for $Y \in \mathcal{Y}$ and $X \in \mathcal{X}$. Formally, the definition of transfer is given as follows.

Definition 1 (Transfer Learning [3])**.** *Given a source domain $\mathcal{D}_S$ and learning task $\mathcal{T}_S$, a target domain $\mathcal{D}_T$ and learning task $\mathcal{T}_T$, transfer learning aims to improve the learning of the target predictive function $f_T(\cdot)$ in $\mathcal{D}_T$ using the knowledge in $\mathcal{D}_S$ and $\mathcal{T}_S$, where $\mathcal{D}_S \neq \mathcal{D}_T$, or $\mathcal{T}_S \neq \mathcal{T}_T$.*

Three major works [3], [10], [11] review the state of the art of transfer learning in classification, regression, unsupervised and reinforcement learning. When dealing with a transfer learning problem, the main questions to answer are: *what to transfer*, *how to transfer* and *when to transfer*. The question of *when to transfer* is mainly related to the issue of avoiding negative transfer, which is when transfer learning has a negative impact on target learning. The literature is primarily focused on the first two questions. For the purpose of studying *what to transfer*, we will use to the categorization done by [3], where transfer learning can be divided into:

- Inductive: Different source and target tasks.

- Transductive: Similar source and target tasks but different source and target domains.
- Unsupervised: Different source and target tasks and different (but related) source and target domains.

To answer the question *how to transfer*, the most common transfer learning approaches are:

- Instance transfer: It can be applied to inductive and transductive learning. In this approach, labeled samples in the source domain are reweighted and used in the target domain [12], [13], [14].
- Feature transfer: It is applied to inductive and transductive learning. It aims at finding a "good" feature representation that can minimize the domain difference, as proposed in [15], [16].
- Parameter transfer: It is mostly applied to solve inductive and transductive transfer learning problems. It works under the assumption that individual models for related tasks share parameters or a combination of hyperparameters [17], [18].
- Relational knowledge transfer: It is mostly used to solve inductive transfer learning problems. It is applied to problems where there is some kind of relation in the data (e.g. network or social network data) [19], [20].

C. Applications of Transfer Learning

Some of the areas where transfer learning has been successfully applied are computer vision, natural language processing and speech recognition [3]. Due to recent advances in the field of deep learning, recent approaches combine deep and transfer learning. For instance, in [21] mid-level image representations learned with convolutional neural network (CNN) are transferred to other visual recognition tasks. The same idea is followed in [22] for character recognition from Latin to Chinese. However, the applications of transfer learning in the field of wireless and mobile networks are still limited. Work has been done for localization by transferring knowledge across devices, time and space via hidden Markov models (HMMs) in [23], [24], [25]. More recently, transfer learning has been applied to caching [26], resources optimization [27], and fault classification [28]. The former two use *feature transfer* frameworks based on collaborative filtering and Q-learning, respectively, while the latter applies *instance transfer*.

D. Motivation of Our Study

Our work shares the same research objectives of the work on tilt-dependent radio map prediction (Section II-A), but with one fundamental difference: in all the aforementioned works the domain of the data used for predicting the signal strength is similar (or even the same) as the target domain. For example, the signal strength radio map of an antenna under a given tilting configuration is interpolated or predicted by using available signal strength samples collected for the same antenna in the same tilting configuration. Instead, we analyze the case where the performance of the target antenna configuration is predicted using training data related to a different tilt configuration. In our previous work [1], we have investigated the dependency between the transferability of the knowledge and the domain difference, when considering the task of tilt-dependent radio map prediction and by using standard machine learning tools. In this work, we aim to solve a similar problem, but with improved performance, by applying transfer learning and exploiting different data sources as training domain.

From the point of view of transfer learning (Section II-B), our work mainly falls into the category of *transductive learning* ($\mathcal{T}_S = \mathcal{T}_T$ and $\mathcal{D}_S \neq \mathcal{D}_T$), when using real measurements for training (Section V-A). However, it is closer to inductive learning ($\mathcal{T}_S \neq \mathcal{T}_T$), when exploiting artificially generated data (Section V-B). Furthermore, our solution is inspired by the *feature transfer* and *parameter transfer* approaches introduced in [21]. The authors propose to extract some internal layers from a CNN, trained with sufficient data collected from the source domain. They add an adaptation layer to correct the difference between distributions in the source and target domain. The resulting network is finally trained with a limited amount of data in the target domain. However, unlike the approach proposed in [21], we do not use a CNN, due to the scarcity of collected data. Instead, we take the internal layers of a fully connected feed-forward neural network (FFN), trained in a given tilt configuration (source domain), and add a new layer. We retrain the final network on a new tilt configuration (target domain). To exploit parameter transfer, we assume that different domains (tilt configurations of the same antenna) share the same combination of hyperparameters (same neural network architecture). In addition, we evaluate the suitability of our approach when using artificially generated data as source domain and quantify the minimum amount of labeled data required from the target domain to carry out predictions. To the best of our knowledge, this is the first work using neural networks

for feature transfer as well as parameter transfer in the area of wireless and mobile networks.

III. Problem Statement and Dataset

In this paper, we address the following problem in mobile radio networks: "*how to predict the performance of a given network configuration by leveraging performance information of different network configurations*". The performance measure that we target is the received signal strength in the downlink. The network configuration domains include the tilting configurations of the transmitting BSs.

We consider a BS that can work in H different tilt configurations, indexed by $h = 1, \ldots, H$. Let $s_h(\mathbf{x}_i)$ be the measured signal strength received at location $\mathbf{x}_i = \{y_i, z_i\}$ when the h-th tilt configuration is selected at the BS, where y_i and z_i indicate the latitude and the longitude of the i-th location, respectively. Let $\mathcal{M}_h$ be the set of location indexes where measurements have been taken with configuration h.

The problem at hand can be defined as follows: given $\{s_h(\mathbf{x}_i) : i \in \mathcal{M}_h\}$, estimate the unknown signal strength $\hat{s}_n(\mathbf{x}_j)$ at the same or different locations, $\mathbf{x}_j$, with $j \in \mathcal{M}_n$, under different network configuration domains, $n \neq h$.

A. Data Collection

The dataset used in this work is composed of reference signal received power (RSRP) outdoor measurements collected in Espoo, Finland, in November 2016 from two commercial LTE BSs with three different 120° sectors each and operating at 2.6 GHz (see Figure 1 reporting the positions of the two antennas and the representation of the target area). Namely, the measurements are collected from three different physical cell identifiers (PCIs), which will be referred to as PCI 1, 2 and 3. PCIs 1 and 2 refer to two different sectors of the same base stations, whereas PCI 3 is a sector of a totally different base station.

The RSRP measurements were collected using an Android device equipped with an application capable of storing the RSRP from all the received cells, the cell identifier, the global positioning system (GPS) position of the device and the timestamp. Such measurements were carried out at a frequency of 1 Hz while walking along routes of 8 km within each cell coverage area, with a minimum and maximum distance from the BS of 30 m and 900 m, respectively. By design, the testing paths were planned to include different propagation conditions: university campus

Fig. 1: Map showing the BS positions and the PCIs (sectors) in the reference dataset

PCI	Electronic tilt setting (in degrees)
1	0, 2, 3, 4, 6
2	0, 2, 3, 6
3	2, 3, 6

TABLE I: Available down-tilt configurations

with two- or three-story buildings, residential areas, parking lots, lower density rural and open area with different types of roads (e.g., pedestrian, cycling and main roads). Each testing path was walked once for each electronic tilt setting. The different tilt configurations are shown in Table I. The receiver was placed at the height of 1.5 m and always kept at the same orientation. The weather conditions were stable and cloudy and the route was covered by snow for most of the measurement campaign.

B. Data Preprocessing

In total, about $3 \cdot 10^5$ RSRP measurements were obtained. Each observation contains the following fields:

- Measurement position (latitude and longitude coordinates)
- RSRP value (downlink signal strength)
- PCI (physical cell identifier)
- Timestamp (date and time)

The raw dataset was preprocessed to remove corrupted samples: for example, at the beginning of each experiment the GPS receiver requires some initialization time during which position

is recorded incorrectly. Moreover, we overlaid the considered area with a grid. For each grid element of size 20 m $\times$ 20 m, we replaced the RSRP values with their average. After the preprocessing steps, the reduced dataset consisted of ~$3.5 \cdot 10^3$ observations per PCI and per tilt configuration, for a total of ~$5 \cdot 10^4$ measurements.

In our previous work [1], we analyze the transferability across different tilt settings of the same PCI as well as the transferability across different PCIs. In particular, we show that the transferability within the same PCI is much stronger than the transferability across different PCIs. Therefore, we focus hereafter on the task of transferring the knowledge from one tilt configuration to another within the same PCI, namely PCI 1. Figure 2 shows a representation of the data collected for different tilt configurations of PCI 1. Figures 2a, 2c, 2e show RSRP values over the considered geographic area, when the antenna was tilted at 2, 3 and 6 degrees, respectively. It can be observed that the spatial distribution of the data follows a similar pattern for different tilt configurations of PCI 1. For example, points located in the main direction of the antenna have higher signal strength values than the rest of the points. In addition, points closer to the antenna also follow a similar pattern, while points far apart have lower RSRP values. Figures 2b, 2d, 2f show the distribution of the data for different tilt configurations and different features (azimuth, distance and RSRP). We observe some similarities between data collected from different tilt configurations. Intuitively, there is a relationship between the data distributions of different tilt configurations (source and target domains). The distance and azimuth distributions are slightly left-skewed in all cases. However, in our case, the data does not come from the same distribution, violating the main assumption of traditional machine learning algorithms. For example, the azimuth distribution for a greater tilt value (Figure 2f) has a lower standard deviation than the distributions for lower tilt values (Figures 2b and 2d).

IV. Prediction Approaches

In this section, we describe our proposed approach for prediction of tilt-dependent radio map as well as the baseline approach used for comparison. Given the antenna location $\mathbf{x}_A$, let $\mathbf{x}$ and h be the target position and the configured antenna tilt, respectively. The following set of features, derived from $(\mathbf{x}, h)$ and shown in Figure 3, is considered for the prediction task:

- the *tilt* configuration of the antenna, $\alpha_A := h$
- the physical *distance* between the antenna and the measurement position, $d(\mathbf{x}) := d(\mathbf{x}, \mathbf{x}_A)$

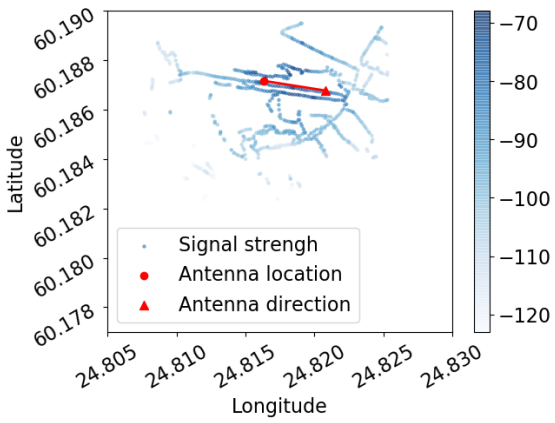

(a) Radio map: PCI 1, Tilt 2

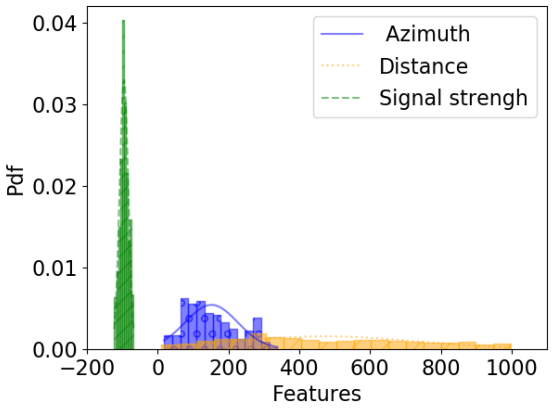

(b) Data distribution: PCI 1, Tilt 2

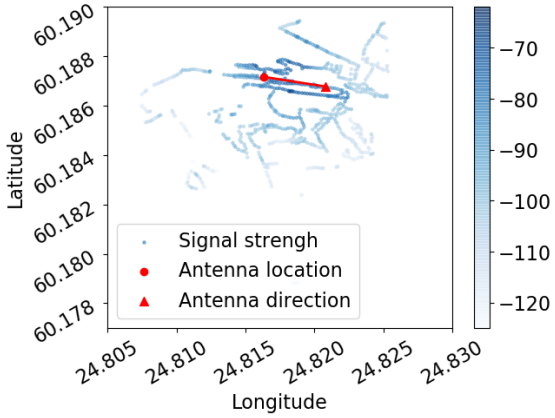

(c) Radio map: PCI 1, Tilt 3

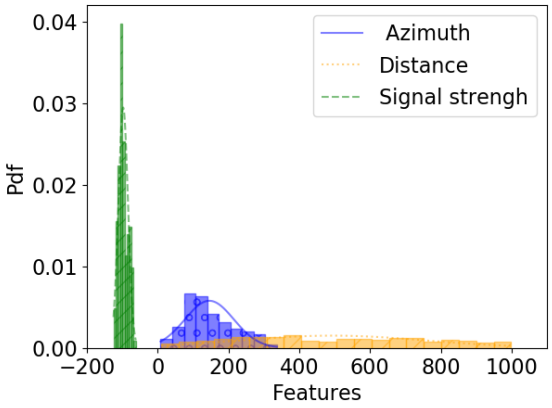

(d) Data distribution: PCI 1, Tilt 3

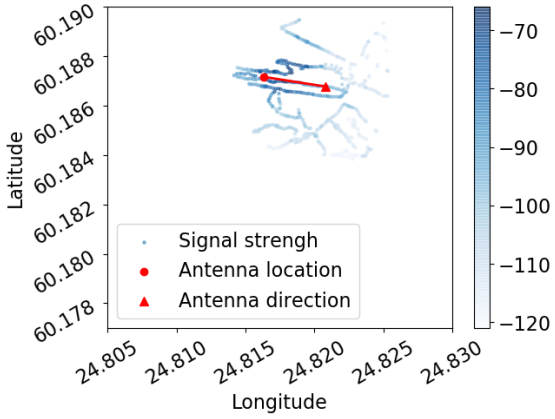

(e) Radio map: PCI 1, Tilt 6

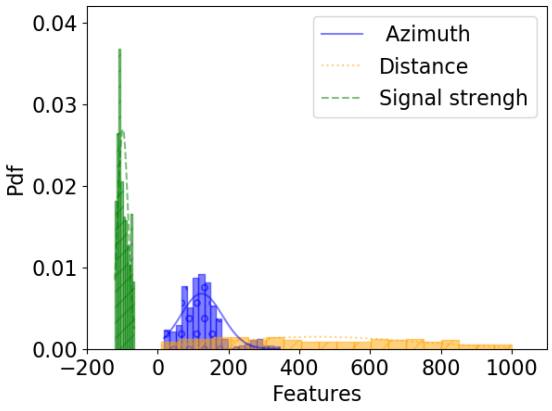

(f) Data distribution: PCI 1, Tilt 6

Fig. 2: Tilt-dependent radio maps and corresponding data distributions

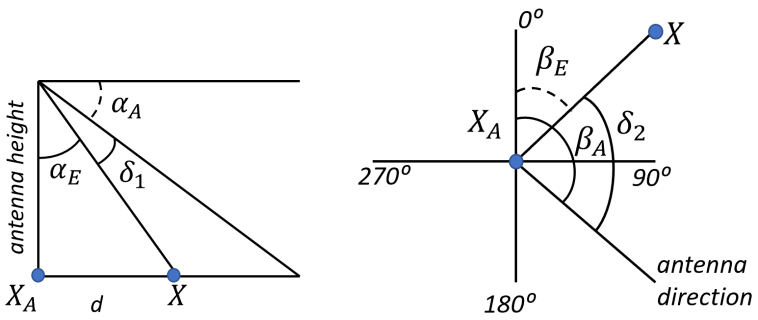

(a) Relative distance (b) Relative azimuth

Fig. 3: Relative angles on the vertical (left) and horizontal (right) planes between the antenna pointing direction and the direction towards the test position $\mathbf{x}$

- the *relative elevation angle* between the down-tilt of the antenna and the vertical direction from the antenna emitting element to the measurement position, defined as:

$$\delta_1(h, \mathbf{x}) = 90° - (\alpha_A + \alpha_E(\mathbf{x}, \mathbf{x}_A)) = 90° - (h + \alpha_E(\mathbf{x}, \mathbf{x}_A)), \tag{1}$$

  where h is the antenna down-tilt (mechanical plus electrical) and α_E is the angle at which the antenna "sees" the target position depending on the antenna position $\mathbf{x}_A$ and the target location $\mathbf{x}$

- the *relative azimuth* between the horizontal orientation of the antenna and the horizontal direction to the measurement position defined as:

$$\delta_2(\mathbf{x}) = \beta_A - \beta_E(\mathbf{x}, \mathbf{x}_A), \tag{2}$$

  where β_A denotes the horizontal orientation of the antenna and β_E is the horizontal orientation of the target position with respect to the antenna position

Each sample in the training dataset is, therefore, associated with a tuple of values (d, δ_1, δ_2). The logarithm transformation is applied to d since the RSRP values are measured in dBm. Finally the feature vector $[d(\mathbf{x}), \delta_1(\mathbf{x}, h), \delta_2(\mathbf{x})]^T$ is obtained and used as input to our models.

A. Deep Transfer Learning

In this section, we describe the proposed transfer learning approach as well as all the optimization steps taken to find the best combination of hyperparameters to tune the algorithms.

The proposed learning approach has been inspired by the fields of computer vision and natural language processing [21] [22], where deep neural networks constitute the performance benchmark for classification and prediction tasks. The core idea of our approach is to train a neural network for the signal strength prediction task in a source domain (reference tilt configuration) and then "wisely" build a new neural network to obtain fine-grained predictions in the target domain (target tilt configuration). The reference neural network architectures used in our approach are FFNs, which are well-known for being powerful nonlinear function approximators [29]. We opt for FFNs instead of more complex network architectures, such as CNNs or recurrent neural networkss (RNNs), since the latter usually requires a big amount of data to avoid overfitting, while FFNs work well also with limited amount of labeled data, which is our case.

We use the mean square error as loss function, which is the common loss used for regression tasks. By using FFNs as the basic building blocks of our architecture, the flow of information only travels forward and the layers of the network are fully connected. Formally, FFN learns a combination of parameters to find the best function approximation. In our case, we aim at finding a set of parameters $\boldsymbol{\theta}$ for the hidden layers and a set of parameters $\mathbf{w}$ for the output layer to estimate $\hat{s}(\mathbf{x})$ for $\mathbf{x} \in \mathbb{R}^p$, as shown in Eq. (3):

$$\hat{s}(\mathbf{x}) = f(\mathbf{x}; \boldsymbol{\theta}, \mathbf{w}) = \boldsymbol{\phi}(\mathbf{x}, \boldsymbol{\theta})^T \mathbf{w} \tag{3}$$

where $\boldsymbol{\phi} : \mathbb{R}^p \rightarrow \mathbb{R}^q$ is a nonlinear transformation defining the hidden layers, and parameters $\mathbf{w} \in \mathbb{R}^q$ map from $\boldsymbol{\phi}$ to the desired output.

The proposed learning approach is composed of the following:

- $\mathcal{D}_S$: the source domain, it consists of the feature space of the reference tilt configuration and its marginal probability distribution
- $\mathcal{D}_T$: the target domain, it consists of the feature space of the target tilt configuration and its marginal probability distribution
- $\mathbf{M}_S = \hat{f}_S(\cdot)$: an FFN with n layers approximating the predictive function in the source domain $f_S(\cdot)$
- $\mathbf{M}_T = \hat{f}_T(\cdot)$: an FFN with m layers approximating the predictive function in the target domain $f_T(\cdot)$
- $\{\mathbf{p}_1, ..., \mathbf{p}_K\}$: the best combination of hyperparameters shared by both FFNs associated with

Number of epochs	500
Batch size	128
Number of inputs	3
Number of layers	4
Hidden units per layer	4, 10, 4, 1
Activation function	Sigmoid
Optimizer	Adam
Learning rate	0.099

TABLE II: Hyperparameters found by Bayesian optimization

the source and target domains respectively[1]

The steps of our transfer learning algorithm are defined as follows:

1) We select the source domain $\mathcal{D}_S$ and we train $\mathbf{M}_S$ on $\mathcal{D}_S$ finding the best combination of hyperparameters $\{\mathbf{p}_1, ..., \mathbf{p}_K\}$ by using Bayesian optimization [30], proved to be an effective way of finding a suboptimal solution in less time, when compared to random search [31], for example. The problem of choosing the hyperparameters is modeled as a sample of a Gaussian process (GP). We start with an initial combination of hyperparameters and dynamically update the searching space based on the built surrogate probability model mapping from hyperparameters to the probability of a score on the objective function. Numerical results show that this process converges in ~50 iterations. Table II shows the optimized combination of hyperparameters as well as the rest of the architecture selected. Then $\mathbf{M}_S$ is trained on $\mathcal{D}_S$ with the chosen hyperparameters. During this process, the model is shown to achieve good performance in the source domain. Figure 4 shows the training and cross validation errors after training for 500 epochs. It can be observed that the training and cross validation errors decrease dramatically during the first 200 epochs. After this they keep decreasing steady. We note that both errors are close to each other, meaning that our model is not overfitting.
2) Once we have obtained $\mathbf{M}_S$, we model $\mathbf{M}_T$ by taking the first $i \leq n$ layers of $\mathbf{M}_S$ with the associated weights and adding new $j \leq m$ layers that are initialized with random weights.

[1]For parameter transfer we assume that the models for source and target domains share a combination of hyperparameters.

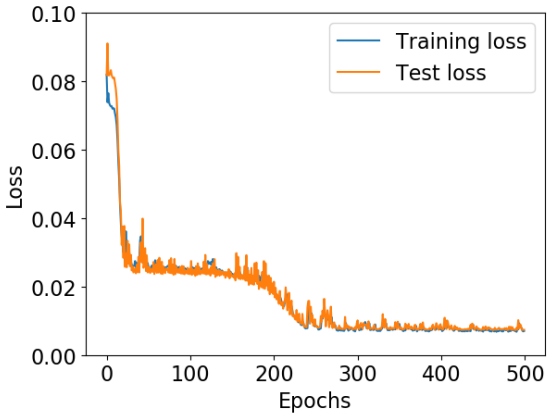

Fig. 4: Learning curve on the source domain

The intuition behind this is that the first layers of the network can capture more general characteristics about the feature space, while the last ones capture more specific behavior.

3) Finally, we train $\mathbf{M}_T$ on $\mathcal{D}_T$ using the hyperparameters $\{\mathbf{p}_1, ..., \mathbf{p}_K\}$ mentioned before. There are two ways of doing this:
   a) We freeze the first i layers and retrain only the last j layers of $\mathbf{M}_T$ on data from $\mathcal{D}_T$. We refer to this approach as DNN.
   b) We retrain all the $i + j$ layers, but at a slower learning rate. By doing this the weights of the first i layers of $\mathbf{M}_T$ are preserved, since they are already good for the classification task in $\mathcal{D}_S$. After back-propagation, these weights are adjusted to better fit the classification task in $\mathcal{D}_T$. We refer to this approach as P-DNN.

Figure 5 shows a graphical representation of $\mathbf{M}_S$ and $\mathbf{M}_T$, where $\mathbf{M}_T$ contains the first three layers of $\mathbf{M}_S$ and two new layers.

We use the Keras framework [32] on top of TensorFlow [33], due to its flexibility for implementing this transfer learning approach and performing hyperparameters search. In total, the training and testing phases of the two models do not last more than two minutes. We use a laptop with 16GB of RAM memory and 7th generation, Intel Core i7 processor.

B. Baseline Methods

In this section, we describe two baseline methods used to benchmark our work: k-nearest neighbors (k-NN) and random forest (RF). Based on our previous work [1], these methods

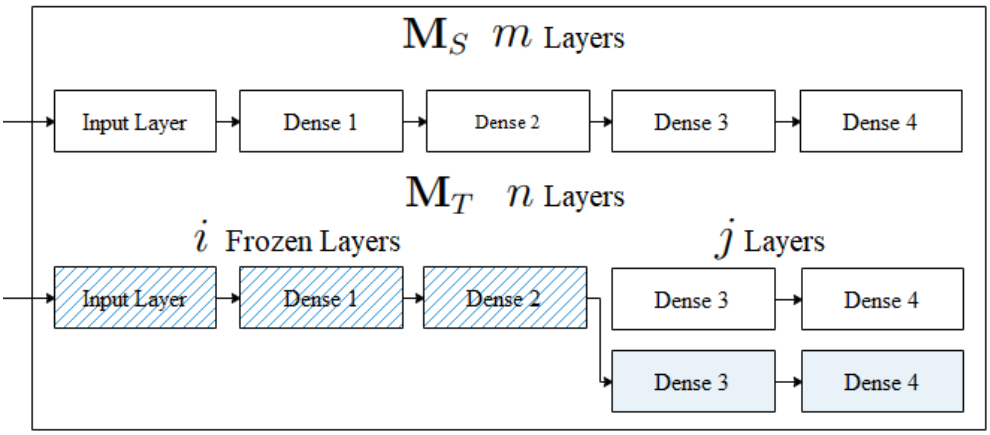

Fig. 5: Transfer learning model

perform the best.

1) k-Nearest Neighbors with Inverse Distance Weighting: This technique extends the classical nearest neighbor approaches [34], and predicts the signal at an unknown target location as a weighted average of the signals at the k closest known locations:

$$\hat{s}(\mathbf{x}) = \sum_{i \in \mathcal{M}(\mathbf{x})} \omega_i s(\mathbf{x}_i). \tag{4}$$

The set $\mathcal{M}(\mathbf{x})$ includes the indexes of the k locations which are geographically closest to the unknown target location $\mathbf{x}$. Weights ω_i are chosen to be inversely proportional to the distance $d(\mathbf{x}_i, \mathbf{x})$ and their sum is normalized to one, that is:

$$\omega_i = \frac{d(\mathbf{x}_i, \mathbf{x})^{-1}}{\sum_{j \in \mathcal{M}(\mathbf{x})} d(\mathbf{x}_j, \mathbf{x})^{-1}}. \tag{5}$$

2) Random Forest: *RF* is one of the ensemble methods used for classification and regression purposes. The algorithm introduced by Ho [35] in 1995, and later extended by Breiman and Cutler [36], uses the idea of bagging to perform predictions. During the process several trees are grown independently using different bootstrapped samples of the data and majority voting or averaging is used for the final prediction. In contrast to traditional trees, the variable used to perform the split in each node is chosen randomly from a set of predictors [36]. RF is known to sometimes outperform other machine learning techniques, such as neural networks, due to its resistance to overfitting [37].

V. EXPERIMENTS

In this section, we describe the set of experiments carried out. We establish a set of metrics to measure the performance and the similarity between source and target domains. We compare the prediction error of our transfer learning method, described in Section IV-A, and the two baselines methods, described in Section IV-B. We perform these experiments with data coming from two different sources: (i) real measurements (Section V-A) and (ii) artificially generated (Section V-B). In both cases we vary the number of instances taken from the target domain. For the DNN and P-DNN this is the number of samples used to train $\mathbf{M}_T$. For the k-NN and RF this is the number of instances added to the source domain for training. The general objective is to map the amount of labeled data required from the target domain and corresponding performance, assessed in terms of mean absolute percentage error (MAPE), which is defined as:

$$\text{MAPE} = \frac{100}{k} \sum_{i=0}^{k-1} \left| \frac{s_i - \hat{s_i}}{s_i} \right|, \tag{6}$$

where k is the number of target positions in the testing dataset.

In the following sections we will discuss the *degree of similarity* between different domains (i.e. datasets). We quantify similarity in terms of Kullback-Leibler (KL) divergence index [38], which measures the relative entropy of a given probability distribution with respect to another one. Namely, given two reference datasets, one used for training and one used for testing, we derive the KL divergence indexes of the probability distributions of the logarithm of the distance (d), relative angle (δ_1) and relative azimuth (δ_2) of the two datasets. For example, the symmetric KL divergence index of the distance probability distributions, in one training and one testing dataset, is given by:

$$D_{KL}(d) = \sum_{i=1}^{k} P_d^{(\text{tr})}(i) \log \frac{P_d^{(\text{tr})}(i)}{P_d^{(\text{te})}(i)} + \sum_{i=1}^{k} P_d^{(\text{te})}(i) \log \frac{P_d^{(\text{te})}(i)}{P_d^{(\text{tr})}(i)}, \tag{7}$$

where $P_d^{(\text{tr})}(i)$ and $P_d^{(\text{te})}(i)$ with $i = 1 \dots k$ defining the discrete probability distributions of the distance in the training and testing dataset, respectively. Similar definitions hold for the KL divergence indexes related to the relative angle δ_1 and relative azimuth δ_2. Finally, to give a more succinct representation of domain similarity, we introduce the domain distance (DD) measure by summing the three indexes together:

$$\text{DD} = D_{KL}(d) + D_{KL}(\delta_1) + D_{KL}(\delta_2). \tag{8}$$

		Training		
		2	3	6
Testing	3	0.21	0	2.58

TABLE III: Domain Distance for different training and testing domains

Table III shows the domain similarity for the different combinations of training and testing domains considered hereafter. Smaller DD values indicate higher domain similarity and vice versa. For instance, when using data from tilt 2 to predict 3, the domains are more similar than when using data from tilt 6 to predict 3.

A. Real Measurements

We use a dataset obtained under a given tilt setting (source domain) to predict the performance of the same antenna under a different tilt configuration (target domain). This falls into the category of *transductive learning*, since the distribution of the data for source and target domains is different ($\mathcal{D}_S \neq \mathcal{D}_T$). Figure 6 shows the results in terms of MAPE, obtained by the different prediction approaches described in Section IV, when considering PCI 1 and different combinations for the training and testing tilt conditions. Figure 6a refers to the case where the training set is obtained with an antenna tilt of 2 degrees and the tilt configuration for the test set is 3 degrees (i.e. we want to predict the radio map at 3 degrees, given the one at 2 degrees). Figure 6b shows the case where the training set is obtained with an antenna tilt of 6 degrees. The same 3 degrees tilt configuration is used for testing in both experiments.

From the results in Figure 6, we can make the following observations:

- The prediction error is impacted by the amount of samples taken from the target domain. In particular, the amount of data taken from the target domain can be decreased by up to 90% with a maximum increase in error rate of 2%. It is worth noting that if no data is taken from the target domain, the baseline and transfer learning approaches must be used under the assumptions of traditional machine learning, where source and target domain are similar. As this is not the case, there is a sharp increase in the error rate of predictions. This justifies the need to model our problem under the framework of transfer learning in order to decrease the prediction error.

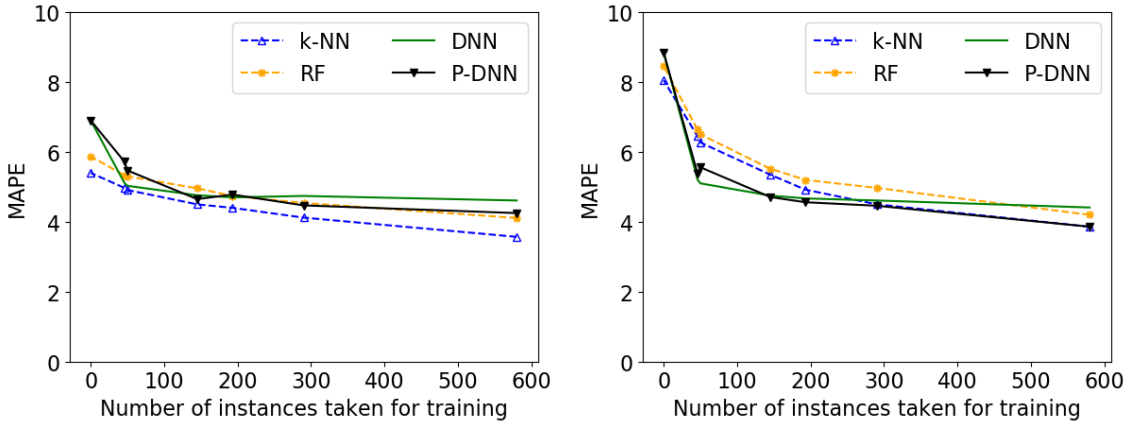

(a) Training tilt 2, testing tilt 3

(b) Training tilt 6, testing tilt 3

Fig. 6: MAPE training on real measurements

- Notably, the baseline methods (k-NN and RF) perform similarly to the transfer learning approaches (DNN and P-DNN) when the source and target domains are similar ($DD = 0.21$ Table III), and when the amount of samples taken from the testing set is greater than 50% (300 instances out of 590). Whereas transfer learning approaches have better performance when the difference among domains increases ($DD = 2.58$ Table III) and the amount of points taken from the testing set is smaller than 200. This is because, transfer learning approaches better capture the physical properties of channel propagation. Thus, being more robust against the cross-domain missing information.
- When the amount of samples taken from the target domain for training is less than 200, DNN outperforms P-DNN; meaning that for a smaller amount of points taken from the target domain retraining the first layers of the network (DNN) is not required. For more than 200 points retraining the whole network (P-DNN) decreases the error.

Similar results have also been obtained for other PCIs and tilt configurations, but they are not reported here for the sake of brevity.

In conclusion, when using real measurements the proposed approach shows benefits compared to the benchmark methods when there is significant difference between source and target domains and when the available samples of the target domain data are limited. In contrast, considerable gains are achieved when introducing artificially generated data. This is discussed in the next

section.

B. Artificial Data

The generation of artificial data, especially for the purpose of data augmentation, has been shown to be successful in the area of computer vision. By augmenting an existing dataset with new data that follows the same distribution as the data used for training, overfitting can be reduced [39]. In our case, we take inspiration from the idea of generating artificial data but instead of augmenting our dataset, we evaluate the gains of performing transfer learning from a dataset artificially generated for a given tilt configuration to a dataset of real measurements. This can be considered as *inductive learning*, because the antenna profile provided by the manufacturer (serving as predictive model in source domain $f_S(\cdot)$) is usually different from the radio propagation model in a particular real environment (the predictive model in target domain $f_T(\cdot)$). Therefore, the source and target tasks are different ($\mathcal{T}_S \neq \mathcal{T}_T$).

To generate our artificial dataset, we create a feature vector by generating different sets of locations at a given tilt configuration. We extract the labels (RSRP values) from the data sheets provided by the antenna manufacturer. Specifically, we create the feature vector by generating the artificial points in two different ways: (i) we reuse the same set of locations that we already have for the different tilt configurations or (ii) we generate a random set of locations no further than 900m from the reference PCI. After generating our set of locations, for each sample we calculate *distance*, *relative angle* and *relative azimuth* (Section IV). Finally, we use the data-sheets provided by the antenna manufacturer to extract the antenna gain on the vertical and horizontal planes. We apply the path-loss model to generate the final set of labels. Formally, the process is defined as follows:

1) Given $\mathcal{M}^h$ as the set of location indexes where measurements for the considered base station running configuration h have been taken, we calculate for each location $\mathbf{x} \in \mathcal{M}^h$ a tuple of values (d, δ_1, δ_2). Then we create the feature vector $[d(\mathbf{x}), \delta_1(\mathbf{x}, h), \delta_2(\mathbf{x})]^T$ as shown in Section IV.
2) Let $\eta(\mathbf{x})$ and $\gamma(\mathbf{x})$ be the horizontal and vertical gain of the antenna in dB respectively, as taken from the manufacturer antenna sheets. Given the known position $\mathbf{x}$, we formally define $\Delta(\mathbf{x})$ as:

$$\Delta(\mathbf{x}) = \eta(\mathbf{x}) + \gamma(\mathbf{x}) \tag{9}$$

3) Given $\Delta(\mathbf{x})$, we use the pathloss model to generate the labels, $\hat{s}(\mathbf{x})$, by applying the following:

$$\hat{s}(\mathbf{x}) = \phi_0 + \phi_1 10\log(d(\mathbf{x})) - \Delta(\mathbf{x}), \tag{10}$$

where ϕ_0 and ϕ_1 are the linear regression coefficients calculated for the reference dataset.

Figure 7 shows the results obtained by the different prediction approaches described in Section IV for PCI 1 and different combinations of training and testing tilt settings. All of them use artificial data as source domain and real measurements as target domain. Specifically, Figures 7a, 7b and 7c refer to the case where the training set is obtained with an antenna tilt of 2, 3 and 6 degrees, respectively, and the tilt configuration for the test set is 3 degrees. Figure 7d refers to the case where the training set is obtained with an antenna tilt of 3 degrees and the same tilt configuration of 3 degrees is used for testing, but the set of locations is randomly generated.

From the results shown in Figure 7, we can make the following observations:

- As in the case of real measurements, the prediction error is impacted by the amount of samples taken from the target domain. However, in case of artificially generated data, there is no cost for the operator. Therefore, there is no limit on the amount of data that can be used for training, especially when the set of locations can be randomly generated.
- Transfer learning outperforms the baselines methods significantly when artificial data is used as source domain. It is worth noting that the only difference with the experiments carried out in Section (V-A) is a change on the conditional probability distribution in the source domain (signal strength values generated artificially). Therefore, transfer learning is better than the baselines methods at capturing the domain difference between the conditional probability distributions in source and target domains.
- When using artificial data as source domain, retraining the network from the first layer (P-DNN) leads to better performance than just retraining the last layers of the network (DNN).
- Using artificial data from the same tilt achieves better performance than using artificial data from different tilt configurations as source domain.

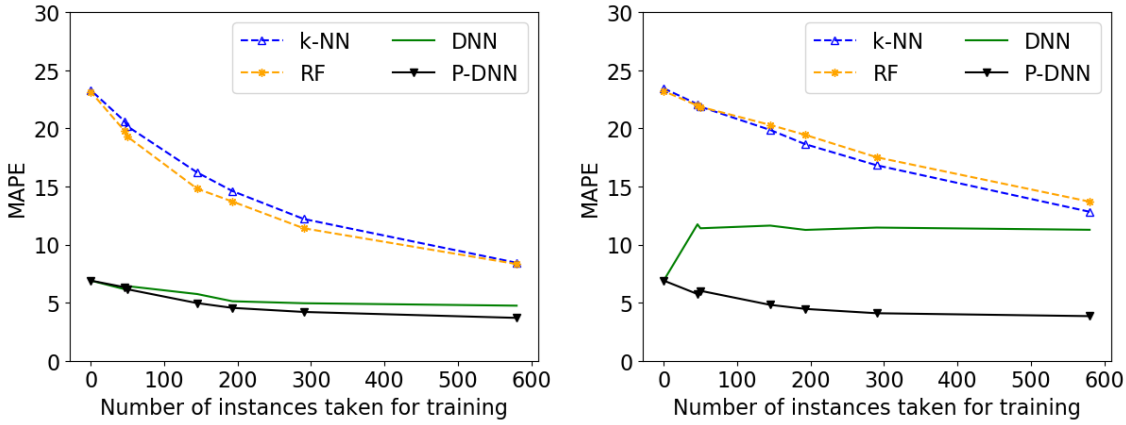

(a) Training on tilt 2, testing tilt 3

(b) Training tilt 3, testing tilt 3

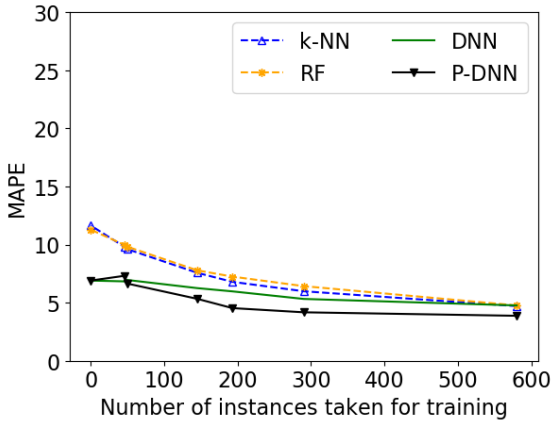

(c) Training on tilt 6, testing tilt 3

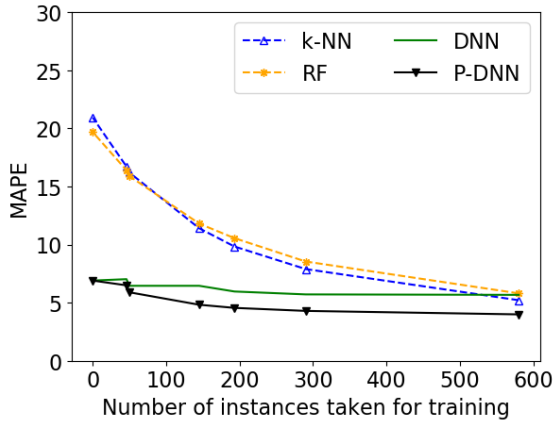

(d) Training on random path tilt 3, testing tilt 3

Fig. 7: MAPE training on artificially generated data

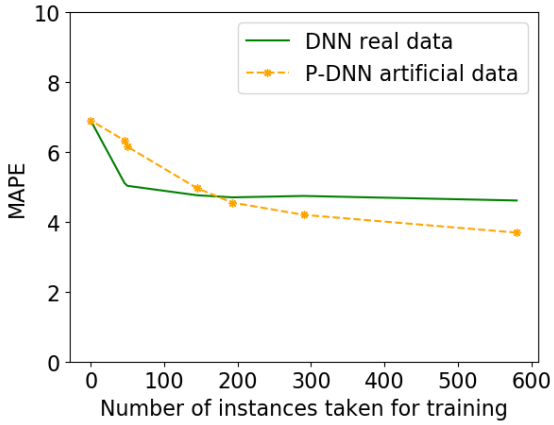

(a) Training on tilt 2, testing tilt 3

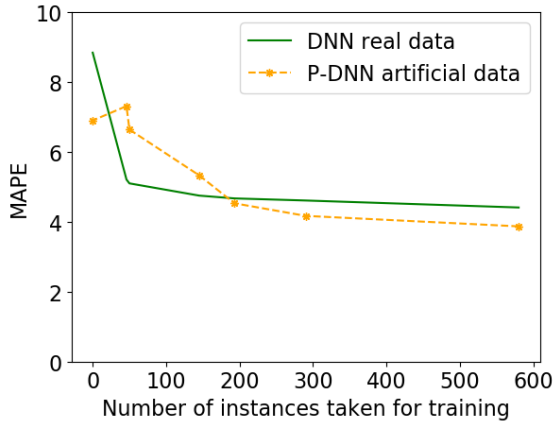

(b) Training tilt 6, testing tilt 3

Fig. 8: MAPE Comparisons between training on real and artificial generated data

To conclude, in Figure 8 we show the best approaches for both artificial data and real measurements to perform radio map prediction. Namely, we consider the prediction of tilt 3 when using tilt 2 and 6 as source domains, for our two different data sources. From Figure 8 we can draw the following conclusions:

- In general, transfer learning using artificial data as the source domain can be used to perform the predictions, since the error rate never exceeds 2%.
- By using transfer learning with artificial data and retraining the network from the first layer (P-DNN artificial data) we can achieve better performance than by using real measurements and not retraining the first layers of the network (DNN real data). This holds when the amount of points taken from the target domain is more than 200. An intuition behind this is that when the dataset is rich enough, the model seems to more easily learn patterns from artificial data than from real measurements. Since real measurements (in our case the signal strength) are affected by noise, errors, obstacles in the terrain, etc.
- Conversely, if the amount of points taken from the target domain for training is less than 200, using real measurements and training just the last layers of the network (DNN real data) leads to better performance than using artificial data and retraining the whole network (P-DNN artificial data).

VI. Conclusions

In this paper, we addressed the problem of predicting the signal strength in the down-link of a real LTE network, where the antennas can be tuned to operate with different antenna tilt configurations. Different approaches were considered as candidates for predicting the signal strength. All of them were based on refined features related to propagation and antenna configuration. As opposed to other works in the field of radio map inference, we studied the quality of prediction of the aforementioned approaches when the datasets used for training and testing are related, but not sampled from the same distribution. We observed that the performance of the predictive models is dependent on the amount of data taken from the testing domain for training. Furthermore, the proposed transfer learning algorithms, based on both feature transfer and parameter transfer methods, are shown to be stable, which means that they are not affected by the domain similarity between source and target domains. Therefore, the learned models can be stored and reused to carry out the predictions for different tilt configurations of the same antenna with larger domain

difference. To reduce the amount of labeled data required from the target domain, we used a dataset of artificially generated measurements. We discussed the suitability of using artificially generated data against real measurements to perform the predictions and we showed that by using transfer learning and artificially generated data the prediction performance decreases at most by 2%, while dramatically reducing the required amount of labeled data. Finally, we provided an analytic method to generate the artificial dataset at zero cost for the operator. Future work will expand on new ways of generating artificial data by using unsupervised learning.

REFERENCES

[1] C. Parera, A. E. Redondi, M. Cesana, Q. Liao, L. Ewe, and C. Tatino, "Transferring knowledge for tilt-dependent radio map prediction," in *Wireless Communications and Networking Conference (WCNC), 2018 IEEE*.

[2] C. Jiang, H. Zhang, Y. Ren, Z. Han, K.-C. Chen, and L. Hanzo, "Machine learning paradigms for next-generation wireless networks," *IEEE Trans. on Wireless Communications*, vol. 24, no. 2, pp. 98–105, 2017.

[3] S. J. Pan and Q. Yang, "A survey on transfer learning," *IEEE Transactions on knowledge and data engineering*, vol. 22, no. 10, pp. 1345–1359, 2010.

[4] J. Moysen, L. Giupponi, and J. Mangues-Bafalluy, "A mobile network planning tool based on data analytics," *Mobile Information Systems*, vol. 2017, 2017.

[5] H. C. Nguyen, I. Rodriguez, T. B. Sorensen, J. Elling, M. B. Gentsch, M. Sorensen, and P. Mogensen, "Validation of tilt gain under realistic path loss model and network scenario," in *Vehicular Technology Conference (VTC Fall), 2013 IEEE 78th*.

[6] C. Phillips, D. Sicker, and D. Grunwald, "A survey of wireless path loss prediction and coverage mapping methods," *IEEE Communications Surveys & Tutorials*, vol. 15, no. 1, pp. 255–270, 2013.

[7] I. Rodriguez, H. C. Nguyen, T. B. Sørensen, J. Elling, M. B. Gentsch, M. Sørensen, L. Kuru, and P. Mogensen, "A geometrical-based vertical gain correction for signal strength prediction of downtilted base station antennas in urban areas," in *Vehicular Technology Conference (VTC Fall), 2012 IEEE*.

[8] D. W. Kifle, B. Wegmann, I. Viering, and A. Klein, "Impact of antenna tilting on propagation shadowing model," in *Vehicular Technology Conference (VTC Spring), 2013 IEEE 77th*.

[9] 3GPP, "Evolved universal terrestrial radio access (E-UTRA); Further advancements for (E-UTRA) physical layer aspects," *TR 36.814, Techincal report*, 2006.

[10] K. Weiss, T. M. Khoshgoftaar, and D. Wang, "A survey of transfer learning," *Journal of Big Data*, vol. 3, no. 1, p. 9, 2016.

[11] M. E. Taylor and P. Stone, "Transfer learning for reinforcement learning domains: A survey," *Journal of Machine Learning Research*, vol. 10, no. Jul, pp. 1633–1685, 2009.

[12] J. Jiang and C. Zhai, "Instance weighting for domain adaptation in nlp," in *Proceedings of the 45th annual meeting of the association of computational linguistics*, 2007, pp. 264–271.

[13] R. Chattopadhyay, Q. Sun, W. Fan, I. Davidson, S. Panchanathan, and J. Ye, "Multisource domain adaptation and its application to early detection of fatigue," *ACM Transactions on Knowledge Discovery from Data (TKDD)*, vol. 6, no. 4, p. 18, 2012.

[14] L. Duan, D. Xu, and I. W.-H. Tsang, "Domain adaptation from multiple sources: A domain-dependent regularization approach," *IEEE Transactions on Neural Networks and Learning Systems*, vol. 23, no. 3, pp. 504–518, 2012.

[15] S.-I. Lee, V. Chatalbashev, D. Vickrey, and D. Koller, "Learning a meta-level prior for feature relevance from multiple related tasks," in *Proceedings of the 24th international conference on Machine learning*. ACM, 2007, pp. 489–496.

[16] M. Long, J. Wang, G. Ding, S. J. Pan, and S. Y. Philip, "Adaptation regularization: A general framework for transfer learning," *IEEE Transactions on Knowledge and Data Engineering*, vol. 26, no. 5, pp. 1076–1089, 2014.

[17] J. Gao, W. Fan, J. Jiang, and J. Han, "Knowledge transfer via multiple model local structure mapping," in *Proceedings of the 14th ACM SIGKDD international conference on Knowledge discovery and data mining*. ACM, 2008, pp. 283–291.

[18] T. Tommasi, F. Orabona, and B. Caputo, "Learning categories from few examples with multi model knowledge transfer," *IEEE transactions on pattern analysis and machine intelligence*, vol. 36, no. 5, pp. 928–941, 2014.

[19] L. Mihalkova, T. Huynh, and R. J. Mooney, "Mapping and revising Markov logic networks for transfer learning," in *AAAI*, vol. 7, 2007, pp. 608–614.

[20] J. Davis and P. Domingos, "Deep transfer via second-order Markov logic," in *Proceedings of the 26th annual international conference on machine learning*. ACM, 2009, pp. 217–224.

[21] M. Oquab, L. Bottou, I. Laptev, and J. Sivic, "Learning and transferring mid-level image representations using convolutional neural networks."

[22] D. C. Cireşan, U. Meier, and J. Schmidhuber, "Transfer learning for Latin and Chinese characters with deep neural networks," in *Neural Networks (IJCNN), The 2012 International Joint Conference on*.

[23] S. J. Pan, J. T. Kwok, Q. Yang, and J. J. Pan, "Adaptive localization in a dynamic WiFi environment through multi-view learning," in *AAAI*, 2007, pp. 1108–1113.

[24] V. W. Zheng, E. W. Xiang, Q. Yang, and D. Shen, "Transferring localization models over time," in *AAAI*, 2008, pp. 1421–1426.

[25] S. J. Pan, D. Shen, Q. Yang, and J. T. Kwok, "Transferring localization models across space," in *AAAI*, 2008, pp. 1383–1388.

[26] E. Başтuğ, M. Bennis, and M. Debbah, "A transfer learning approach for cache-enabled wireless networks," in *Modeling and Optimization in Mobile, Ad Hoc, and Wireless Networks (WiOpt), 2015 13th International Symposium on*. IEEE, 2015, pp. 161–166.

[27] A. Galindo-Serrano, L. Giupponi, and G. Auer, "Distributed learning in multiuser OFDMA femtocell networks," in *Vehicular Technology Conference (VTC Spring), 2011 IEEE 73rd*. IEEE, 2011, pp. 1–6.

[28] W. Wang, J. Zhang, and Q. Zhang, "Transfer learning based diagnosis for configuration troubleshooting in self-organizing femtocell networks," in *Global Telecommunications Conference (GLOBECOM 2011), 2011 IEEE*.

[29] I. Goodfellow, Y. Bengio, A. Courville, and Y. Bengio, *Deep learning*. MIT press Cambridge, 2016, vol. 1.

[30] J. Snoek, H. Larochelle, and R. P. Adams, "Practical Bayesian optimization of machine learning algorithms," in *Advances in neural information processing systems*, 2012, pp. 2951–2959.

[31] J. Bergstra and Y. Bengio, "Random search for hyper-parameter optimization," *Journal of Machine Learning Research*, vol. 13, no. Feb, pp. 281–305, 2012.

[32] F. Chollet *et al.*, "Keras," https://github.com/fchollet/keras, 2015.

[33] M. Abadi, P. Barham, J. Chen, Z. Chen, A. Davis, J. Dean, M. Devin, S. Ghemawat, G. Irving, M. Isard *et al.*, "Tensorflow: A system for large-scale machine learning." in *OSDI*, vol. 16, 2016, pp. 265–283.

[34] T. Cover and P. Hart, "Nearest neighbor pattern classification," *IEEE transactions on information theory*, vol. 13, no. 1, pp. 21–27, 1967.

[35] T. K. Ho, "Random decision forests," in *Document Analysis and Recognition, 1995., Proceedings of the Third International Conference on*, vol. 1. IEEE, 1995, pp. 278–282.

[36] A. Liaw, M. Wiener *et al.*, "Classification and regression by randomforest," *R news*, vol. 2, no. 3, pp. 18–22, 2002.

[37] L. Breiman, "Random forests," *Machine learning*, vol. 45, no. 1, pp. 5–32, 2001.

[38] J. M. Joyce, "Kullback-Leibler divergence," in *International Encyclopedia of Statistical Science*. Springer, 2011, pp. 720–722.

[39] A. Krizhevsky, I. Sutskever, and G. E. Hinton, "Imagenet classification with deep convolutional neural networks," in *Advances in neural information processing systems*, 2012, pp. 1097–1105.

Maximum Throughput Scheduling for Multi-connectivity in Millimeter-Wave Networks

Cristian Tatino*†, Ilaria Malanchini†, Nikolaos Pappas*, Di Yuan* *Department of Science and Technology, Linköping University, Sweden
Email: {cristian.tatino, nikolaos.pappas, di.yuan,}@liu.se †Nokia Bell Labs, Stuttgart, Germany
Email: ilaria.malanchini@nokia-bell-labs.com

Abstract

Multi-connectivity is emerging as promising solution to provide reliable communications and seamless connectivity at the millimeter-wave frequency range. Due to the obstacles that cause frequent interruptions at such high frequency range, connectivity to multiple cells can drastically increase the network performance in terms of throughput and reliability by coordination among the network elements. In this paper, we propose an algorithm for the link scheduling optimization that maximizes the network throughput for multi-connectivity in millimeter-wave cellular networks. The considered approach exploits a centralized architecture, fast link switching, proactive context preparation and data forwarding between millimeter-wave access points and the users. The proposed algorithm is able to numerically approach the global optimum and to quantify the potential gain of multi-connectivity in millimeter-wave cellular networks.

I. Introduction

The fifth generation (5G) of mobile communications is characterized by ambitious requirements to be fulfilled in terms of broadband access, connection density and data rate, e.g., 50 Mbps everywhere and an amount of connections in the order of thousands per km^2 as reported in [1]. Millimeter wave (mm-wave) communications technology is one of the promising solutions to tackle these challenges. Mm-wave increases the available spectrum resources by exploiting

under-utilized frequency bands between 30 to 300 GHz. On the other hand, communication in these frequency bands is subject to more challenging propagation conditions than the lower frequency bands, especially in terms of free space path loss and penetration loss. This latter may lead to frequent transmission interruptions when there is no line-of-sight (LOS). Multi-connectivity (MC) represents a possible solution to minimize the number of communication interruptions, by allowing the users (UEs) to establish and maintain connections with multiple cells/access points at the same time.

The benefits of having multiple links available for a single UE in a mm-wave wireless network are discussed in several works, e.g., [2] and [3]. These show how the MC can improve the mm-wave performance in terms of denial of service, outage and drop session probabilities when multiple mm-wave access points (mmAPs) can simultaneously transmit to the UE. The work in [4] proposes several potential centralized architectures for MC in mm-wave communications. In particular, these are based on a common framework for mm-wave access supported by low band frequencies. The authors in [4] qualitatively analyze the different architectural approaches in terms of required messages and overhead. Moreover, in [5], the authors propose a new alignment procedure, which can represent a bottleneck in a mm-wave MC scenario. The proposed method can reduce the duration of this phase when the UEs sustain connections with multiple mmAPs. The vast majority of the works dealing with MC assume a centralized architecture with accurate synchronization between the network elements, which is also a fundamental requirement for the coordinated multipoint (CoMP) joint transmission method. In particular, the work in [6] proposes a centralized radio-over-fiber architecture for CoMP in mm-wave small cell networks. The analysis and the experimental results show increased performance in reception quality and probability of LOS.

In this work, we consider a two-layer outdoor cellular network consisting of 5G low band base stations (5G-LBs) and mmAPs connected to a network controller (NC). Moreover, by exploiting the synchronization between the mmAPs, we assume that a UE can establish and maintain multiple connections and possibly receive data from several mmAPs at the same time, similar to a CoMP joint transmission approach.

A. Contributions

In a multi-connectivity scenario, one of the most relevant aspects is the link scheduling problem. In this work, we propose a novel link scheduling approach for network throughput

maximization, and quantify the potential gain of MC and CoMP for mm-wave cellular networks. We formulate the optimal link scheduling problem as a binary integer program (BIP) and then, we propose an algorithm for solving the problem, which is able to numerically approach the global optimum. We exploit a fast link switching mechanism based on the assumption that each link can be in one of four different states. These states determine the time needed to the link to establish a connection and start the transmission.

Finally, by using predicted information about the channel quality over a certain time window, the NC optimizes the link scheduling and prepares in advance the UEs and the mmAPs for the communication. We evaluate the performance of the proposed scheduling algorithm with simulations, and we show the advantages with respect to the single connectivity (SC) approach in terms of throughput and number of interruptions. The rest of the paper is organized as follows: in Section II we describe the system model and the assumptions. In Section III and in Section IV we formulate the optimization problem and we present the solution algorithm for the MC approach. Finally, Section V illustrates the results and performance comparison and Section VI concludes the paper.

II. System Model and Assumptions

As in [4], we consider an MC approach for which each UE is associated to a 5G-LB and possibly to several mmAPs, where, the control and the data planes are split and using the 5G-LB and the mmAPs, respectively. The two layers are connected to an NC in a centralized architecture that enables fast link switching, mmAPs data buffer synchronization, data forwarding, and possibly joint transmissions. In this latter case, several mm-wave connections transmit to the UE the same data, combined then at the receiver [6].

Furthermore, we assume that the mmAPs are perfectly synchronized both in frequency and time and the signals arrive to the UE in-phase. The beamforming gain of downlink transmissions at the receiver depends on how the UE and the mmAPs perform beam alignment. For this purpose, both the mmAP and the UE have several sub-arrays and radio frequency (RF) chains such that each of them can perform the beam alignment with a mmAP, independently. Moreover, we consider that the beams are narrow enough so that the interference becomes negligible, as shown in [7], and we assume that the signal is completely blocked in NLOS conditions and the resulting link throughput is zero.

We assume that the NC has the perfect knowledge of the channel quality condition for each UE over a certain upcoming time window in term of both LOS/NLOS states and achievable throughput. In a real scenario these information can obtained by applying several channel quality estimation and prediction techniques. Since, in this work, we are mainly interested to show the potential gain of MC, we do not consider a specific prediction technique, but the NC exploits this information and proactive link preparation, for optimizing link scheduling.

A. Fast Link Switching

As mentioned above, we consider a fast link switching mechanism, based on [4], which exploits different link states. In particular, each link state defines which operations the mmAP, the UE and NC are performing, i.e., UE context transferring, data buffer exchanging and transmission. In this work, we use the term UE context, for both 5G-LB and mmAPs, to refer to the block of information required to maintain the UE connection, as defined in [8]. The UE context is established with a 5G-LB or mmAPs at the first access of a UE as well as when the handover procedure is completed. Hereafter, the following link states are introduced: active (A), hot stand-by (H), cold stand-by (C), and inactive (I).

- The link is in A when the mmAP is transmitting data, received by the NC, to the UE.
- A link is in H when the UE, the mmAP and the NC have completed the UE context preparation. The mmAP is receiving UE data from the NC, but it is not transmitting them, since the beam alignment is not yet performed.
- A link is in C when the mmAP is not receiving data from the NC. The mmAP is performing only the operations needed to obtain the UE context information and the buffering data, which are not received yet.
- A link is in I if it is in none of the above states.

The mmAP consumes power, backhaul capacity, and radio resources (time-frequency slots) in both A and H states. The purpose of introducing four different states is to define the transition of a link from I to A. Namely, each link in I should go through C and H before becoming A. By allowing a link to be prepared in advance, we can reduce the time needed to activate the link when a communication interruption occurs. The transition between H and A can occur only in LOS (since it requires pilot transmission [9]), while, the transition from C to H can be performed in NLOS since the control messages between the NC and UE are transmitted by the 5G-LB. We

refer to the amount of time needed to transit between states as transition time, which depends on the performed operations.

In summary, given the assumptions and the architecture described above, we aim to solve the optimal link scheduling problem in an MC mm-wave cellular network such that, given a certain time window for which the channel quality is known, the network throughput is maximized. The link scheduling problem is subject to the constraints on the transition time between the different link states and the mmAP total power budget. In the following sections, we formulate the optimization problem and present a solution algorithm.

III. Multi-connectivity Problem Formulation

In this section, we formulate the optimization problem introduced in Section II-A. Namely, given a set of mmAPs $\mathcal{M}$, a set of UEs $\mathcal{U}$, and a set of time slots $\mathcal{K}$, with cardinalities M, U and K respectively, the NC decides, for each time slot, which state to assign to each link in order to maximize the network throughput (i.e., the sum of all the UEs' throughput). The relation between the UE's throughput and the corresponding active links is non-linear. To deal with non-linearity, we first introduce the concept of *configuration*, which can be then used to formulate the optimization problem as a linear BIP. A configuration refers to a subset of links whose elements are active and in LOS. Since the channel condition may change over time, for slot k we define the set of all the possible configurations $\mathcal{S}_k$ and denote its cardinality by S_k. Each configuration $s \in \mathcal{S}_k$ defines the achieved network throughput.

Now, given the sets of configurations $\mathcal{S}_k$, the task of the NC is to choose one among the given configurations (at each time slot) in order to maximize the network throughput. As mentioned above, we assume that at each time slot and for each mmAP-UE pair, the NC knows the link status, i.e., whether or not it is in LOS. Therefore, we define the binary parameter l^{ijk}, which is equal to 1 if link ij between mmAP i and UE j is in LOS in time slot k and 0 otherwise. Moreover, since a link can be in several states, as described in Section II-A, we define the mutually exclusive binary variables y_a^{ijk}, y_h^{ijk}, and y_c^{ijk}. They represent the state of link ij in time slot k, and they are equal to 1 when the link states are A, H and C, respectively. When the variables associated to a link in a time slot are all equal to zero, the link is inactive.

Furthermore, we define the variable z^{sk}, with $s \in \mathcal{S}_k$ and $k \in \mathcal{K}$, which is set to 1 if configuration s is used in time slot k and 0 otherwise. Since each configuration defines a subset of active links, we introduce the parameter α^{ijsk}, which is equal to 1 if link ij is active in

configuration s of time slot k. The throughput provided by a configuration s to UE j in time slot k is given by parameter r^{jsk}. This value is known to the NC, because the throughput is fully determined in each configuration. Now, we can formulate the problem as follows:

$$P1: \max_{y_a^{ijk}, y_h^{ijk}, y_c^{ijk}, z^{sk}} \sum_{k=1}^{K} \sum_{s=1}^{S_k} \sum_{j=1}^{U} r^{jsk} z^{sk} \tag{1a}$$

$$\text{s.t.} \sum_{j=1}^{U} (P_a y_a^{ijk} + P_h y_h^{ijk}) \leq P_{tot} \quad \forall i \in \mathcal{M}, k \in \mathcal{K} \tag{1b}$$

$$y_a^{ijk} + y_h^{ijk} + y_c^{ijk} \leq 1 \quad \forall i \in \mathcal{M}, j \in \mathcal{U}, k \in \mathcal{K} \tag{1c}$$

$$\sum_{s=1}^{S_k} z^{sk} \leq 1 \quad \forall k \in \mathcal{K} \tag{1d}$$

$$y_a^{ijk} = \sum_{s=1}^{S_k} \alpha^{ijsk} z^{sk} \quad \forall i \in \mathcal{M}, j \in \mathcal{U}, k \in \mathcal{K} \tag{1e}$$

$$l^{ijn} y_h^{ijn} + y_a^{ijk-1} \geq y_a^{ijk} \tag{1f}$$

$$\forall i \in \mathcal{M}, j \in \mathcal{U}, k \in \mathcal{K}, n \in \{k - t_{ha}, \ldots, k-1\}$$

$$y_c^{ijn} + y_h^{ijk-1} + y_a^{ijk-1} \geq y_h^{ijk} \tag{1g}$$

$$\forall i \in \mathcal{M}, j \in \mathcal{U}, k \in \mathcal{K}, n \in \{k - t_{ch}, \ldots, k-1\}$$

$$y_a^{ijk}, y_h^{ijk}, y_c^{ijk}, z^{sk} \in \{0, 1\} \tag{1h}$$

$$\forall i \in \mathcal{M}, j \in \mathcal{U}, k \in \mathcal{K}, s \in \mathcal{S}_k.$$

The objective function, given by (1a), represents the sum of all the UEs' throughput associated to the selected configurations. The UE's throughput is computed by the well-known Shannon's formula for the AWGN channel capacity. According to the assumptions in Section II, the throughput provided by the s-th configuration at the k-th time slot to the j-th UE can be computed as in [6] :

$$r^{jsk} = B \log_2(1 + \sum_{i=1}^{M} \sum_{j=1}^{U} \alpha^{ijsk} SNR^{ijk}), \tag{2}$$

where, SNR^{ijk} is the signal-to-noise ratio for the link between the i-th mmAP and the j-th UE at the k-th time slot and B denotes the system bandwidth. Constraints (1b) limit the total transmit power per mmAP to be less than or equal to the power budget, where P_a and P_h are parameters that represent the power consumed by a mmAP when a link is A or H, respectively. Inequalities (1c) impose each link to be in maximum one state. Constraints (1d) force the selection

of at most one configuration per time slot, for which the corresponding active links are set by equalities (1e).

Constraints (1f) and (1g) take into account the transition times from state H to A and from C to H, respectively. In particular, link ij can be active in time slot k if either it is A in time slot $(k\text{-}1)$ or it is H for the previous t_{ha} time slots consecutively. This comes from the alignment phase, in which the mmAP and the UE need to be in LOS. Similarly, a link can be in the state H if either it is in the state A or H in time slot $(k\text{-}1)$ or it has been in the state C for t_{ch} time slots.

The optimization problem P1 is not convex since it is a BIP. Moreover, the cardinality of $\mathcal{S}_k$, that is at most 2^{MU}, grows exponentially with the number of UEs and mmAPs. However, most of the configurations are not relevant for constructing the optimal solution. Therefore, we follow an approach similar to the one considered in [10] that is presented in the next section.

IV. Multi-connectivity Optimization Algorithm

In this section, we present an algorithm to solve the problem P1 formulated in Section III and deal with the exponential growth of configurations. The algorithm is based on a column generation approach. Specifically, we consider the continuous relaxation of P1, which is a linear program, and decompose it into a master problem (P2) and a pricing problem (P3). For sake of space we do not explicitly show the formulation of P2, but it can be expressed as P1, with the differences that (a) the constraint (1h) is replaced with $0 \leq y_a^{ijk}, y_h^{ijk}, y_c^{ijk}, z^{sk} \leq 1$ (continuos relaxation) and (b) we consider only a subset of configurations $\breve{\mathcal{S}}_k$. By solving P3, we generate new configurations and associated network throughput that progressively improve the solution of P2.

More precisely, the configurations represent columns in P2 and adding a new configuration is equivalent to adding a new column. We generate a new subset of configurations per each time slot k since the channel conditions, hence the network throughput associated with a configuration, may change over the time slots. The solution of P2 is used by the pricing problem to determine whether a new configuration can improve network throughput or not. The resulting algorithm is depicted in Algorithm 1 and described in details in Section IV-B.

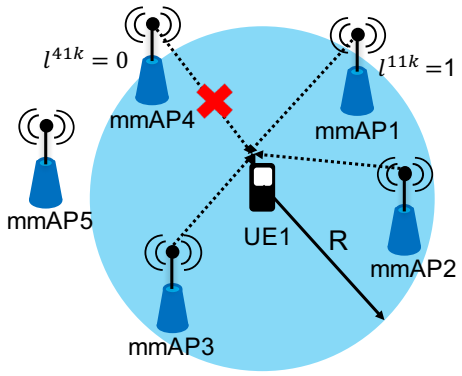

Fig. 1: Possible scenario for the local enumeration. In this case only mmAPs 1, 2 and 3 are considered for UE 1 since mmAP 4 is in NLOS and mmAP 5 is outside the range R, thus, only mmAPs 1, 2, and 3 are included in the set $\mathcal{Q}^{1k}$. Therefore, we have that $E_1 = 2^3$, and the possible combinations are represented by the following sets: $\mathcal{V}^{11k} = \{\}$, $\mathcal{V}^{12k} = \{1\}$, $\mathcal{V}^{13k} = \{2\}$, $\ldots$, $\mathcal{V}^{18k} = \{1, 2, 3\}$.

A. Pricing Problem

In this section, we define the pricing problem for the column (i.e., configuration) generation. Before proceeding with the formulation, we introduce the concept of local enumeration as in [10]. This is needed in order to decrease the complexity of the pricing problem, since for each UE there are 2^M possible configurations of active links, and considering all of them is not scalable. The local enumeration concept is based on the idea that, in each time slot, typically the number of mmAPs, that significantly contribute to the UE's throughput, is small with respect to M. Thus, we define the set $\mathcal{Q}^{jk}$, which contains all the mmAPs that are in LOS and at a maximum distance R with respect to UE j in time slot k. Then, we consider all the possible combinations of the active mmAPs included in the set $\mathcal{Q}^{jk}$, whose number is E_j. Each combination is represented by a set $\mathcal{V}^{jek}$, which contains the active links for UE j in time slot k for combination $e \in [1 \ldots E_j]$. Each set $\mathcal{V}^{jek}$ determines a UE's throughput r^{jek}. Fig. 1 shows an example of local enumeration for UE 1 with some possible combinations of active links.

Now, in order to formulate the pricing problem, we introduce the binary variables α^{ij} and v^{je}. The former is set to 1 if the link between the mmAP i and the UE j is A, and zero otherwise, and it is then used to set the corresponding parameter α^{ijsk} of the master problem (for the considered time slot k and generated configuration s). The latter variable, v^{je} determines which set $\mathcal{V}^{jek}$ is selected among the E_j scenarios for the active links of UE j. Thus, we can formulate

the pricing problem for time slot k as follows:

$$P3: \max_{\alpha^{ij}, v^{je}} \sum_{j=1}^{U} r^j - \sum_{i=1}^{M} \sum_{j=1}^{U} \lambda^{ij} \alpha^{ij} \tag{3a}$$

$$\text{s.t.} \sum_{j=1}^{U} P_a \alpha^{ij} \leq P_{tot} \quad \forall i \in \mathcal{M} \tag{3b}$$

$$\sum_{e=1}^{E_j} v^{je} = 1 \quad \forall j \in \mathcal{U} \tag{3c}$$

$$\sum_{e: h \in \mathcal{V}^{je}} v^{je} \leq \alpha^{hj} \quad \forall j \in \mathcal{U}, h \in \mathcal{Q}^j \tag{3d}$$

$$r^j = \sum_{e=1}^{E_j} v^{je} r^{je} \quad \forall j \in \mathcal{U}. \tag{3e}$$

$$\alpha^{ij}, v^{je} \in \{0, 1\} \quad \forall i \in \mathcal{M}, j \in \mathcal{U}, e \in [1 \dots E_j]. \tag{3f}$$

Expression (3a) represents the objective function, where λ^{ij} are the dual variables associated with constraints (1e) of P2. The dual variables π^{ij}, associated with constraints (1d) of P2, are not explicitly written out, because they are additive constants in the objective function.

Constraints (3b) are related to the total transmit power budget for the mmAPs that is considered also here in order to generate only configurations that are feasible for P2. Equalities (3c) impose that only one combinations of active links is selected per time slot and per UE. The constraints (3d) identify which links must be active according to the selected combinations and state the consistency between the v-variables and α-variables. The equalities (3e) define the UEs' throughput r^j associated with the selected combinations.

B. Algorithm

Finally, the optimal scheduling algorithm is presented in Algorithm 1. At each iteration, Algorithm 1 solves the problem P2 and obtains the dual variables λ^{ij} and π^{ij}, whose values are used to compose the objective function of the pricing problem (3a). Thus, for each time slot, we solve the problem P3 and include the resulting configuration and associated UEs' throughput to the master problem if the reduced cost is positive. The algorithm concludes when none of the remaining configurations, not included in the subsets $\breve{\mathcal{S}}_k$, has positive reduced cost. In this case we solve the binary integer version of P2.

Algorithm 1

Construct P2 with a subset of configurations $\breve{S}_k$
repeat
  for $k \in K$ **do**
    for $s \in S_k \backslash \breve{S}_k$ **do**
      Solve P2
      if $\max_{s \in S_k \backslash \breve{S}_k} \sum_{j=1}^{U} r^{jsk} - \sum_{i=1}^{M} \sum_{j=1}^{U} \lambda^{ijsk} \alpha^{ijsk} - \pi^{ij} > 0$ **then**
        Add the corresponding configuration to $\breve{S}_k$
      end if
    end for
  end for
until $\max_{k \in K} \max_{s \in S_k \backslash \breve{S}_k} \sum_{j=1}^{U} r^{jsk} - \sum_{i=1}^{M} \sum_{j=1}^{U} \lambda^{ijsk} \alpha^{ijsk} \leq 0$
Solve the binary integer version of P2

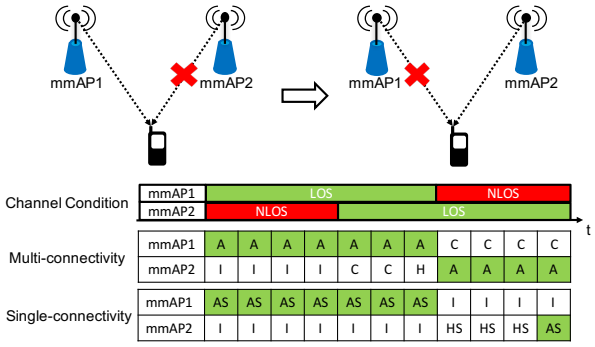

Fig. 2: This figure shows the difference between the link switching of the MC and SC. In the figure, t_s is equal to the sum of t_{ha} and t_{ch}, which in turn are set to 1 and 2 time slots, respectively. For the SC case we define the states AS and HS, which correspond to a link that is active or performing the handover, respectively.

V. Performance Evaluation

In this section, we compare the maximum network throughput achieved by Algorithm 1 ("MC + CoMP") and the solution of the SC approach. For sake of space we do not present the formulation of this latter, which can be written as a linear BIP. More precisely, in the SC case, a UE can be connected only with one mmAP per time slot, which means that the UE can either receive data from or performing the handover with a mmAP. The handover duration is represented by the parameter t_s. In order to make a fair comparison between the MC and the SC cases, also for this latter we assume perfect channel quality prediction. In summary, for the SC case we have that (a) link switching can only start in LOS (there is no support of 5G-LBs) and (b) the UE cannot be connected to the previous mmAP while it is switching to a new one, as shown in Fig. 2.

TABLE I: Simulation parameters.

P_{tot}	30 dBm	P_a	24 dBm	P_h	24 dBm
G_a	15 dBi	G_u	10 dBi	h_{BS}	10 m
h_{ut}	1.5 m	f_c	30 GHz	P_N	-85 dBm
B	1 GHz	K	20	t_{ha}	1
t_{ch}	2	t_s	3	R	360 m

Moreover, we compare these solutions with the network throughput reached by the MC case without CoMP ("MC no CoMP"), in which, differently from the SC case, the UEs can keep the connections with both the 5G-LB and possibly multiple mmAPs. However, for the MC without CoMP case, each UE can have at maximum one active link per time slot. In addition, we report the solution of the master problem P2, once the column generations is ended ("MC + CoMP Bound"), which represents an upper bound of the global optimum of P1.

A. Simulation Setup

We consider an area of 250×250 m^2, where the mmAPs and the UEs are randomly distributed following a uniform distribution. The UEs move following a uniform rectilinear motion with a speed of 3 km/h and a constant direction randomly chosen. Similar to [11], we model the interruption inter-arrivals as independent exponential random variables with parameter λ, while the duration of an interruption is characterized by a uniform distribution between $[400, 1000]$ milliseconds (ms).

In order to compute the throughput associated to a link, we express the SNR in decibel (dB) as follows: $SNR = P_a + G_a + G_u - PL_{UMi-LOS} - P_N$, where G_a and G_u are the beamforming gains of the mmAP and the UE respectively. The term $PL_{UMi-LOS}$ is the path loss, which follows the model for urban micro cells (UMi) in LOS outdoor street canyon environment described in [12]. This depends on the height of the mmAP h_{BS}, the height of the UE h_{ut}, the carrier frequency f_c and the distance between the transmitter and the receiver. P_N represents the noise power.

In order to obtain a comprehensive performance evaluation, hereafter, we vary several parameters, such as M, P_{tot}, and λ. Unless specified otherwise, other parameters are fixed and shown in Table I, where K, t_{ha}, t_{ch}, and t_s are expressed in the number of time slots. More precisely, for t_{ha}, we refer to the values described in [5] for digital beamforming at the mmAPs and analog

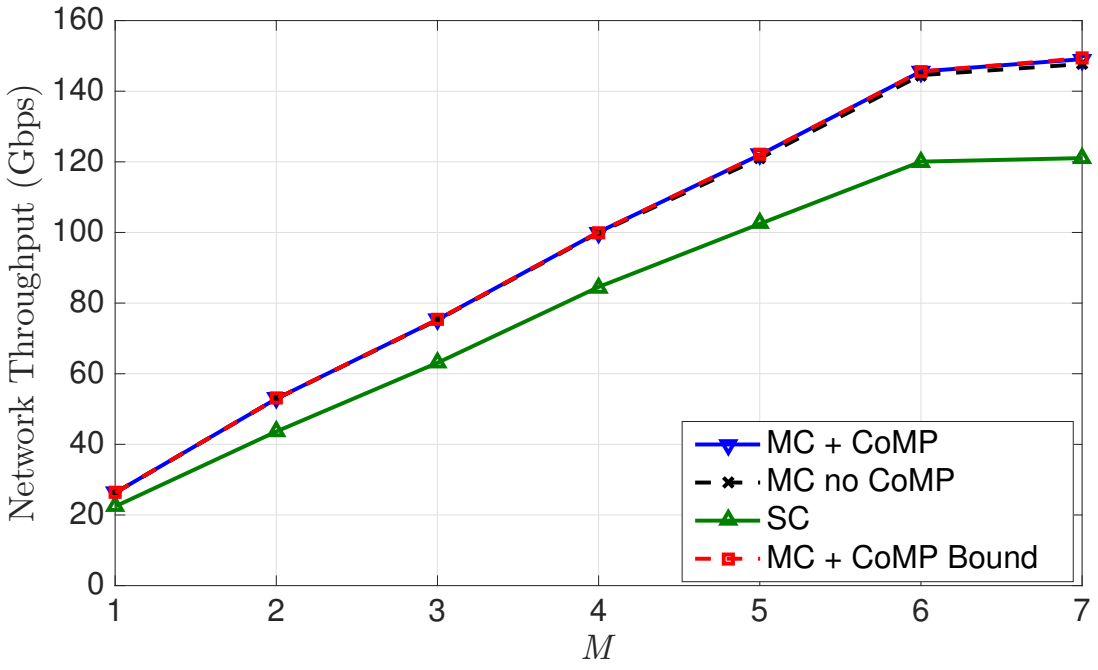

Fig. 3: Network throughput when varying the number of mmAPs M, for U = 20, λ^{-1} = 250 ms.

beamforming at the UEs, with 32 beams at the mmAP and 8 at the UE. Since t_{ha} is the smallest time unit in scheduling, we set the duration of a single time slot equal to t_{ha} and we assume that the channel condition does not change in a time slot. Furthermore, we assume R to be large enough for the considered area, so that all mmAPs can potentially transmit to all UEs.

B. Results

In Figs. 3-5, we compare the network throughput resulting from the MC with and without CoMP, and the SC cases, when varying M, λ and P_{tot}. Note that, given the assumption P_a = P_h, the power budget, P_{tot}, can be expressed in terms of maximum number of simultaneous A and H links per mmAP (4 for $P_{tot} = 30$ dBm). We can observe that Algorithm 1 almost overlaps with the upper bound, which means that, at least for the analyzed cases, the solution of Algorithm 1 is able to numerically approach the global optimum.

Specifically, Fig. 3 shows the network throughput when varying the number of mmAPs M. The number of UEs is U = 20 and λ^{-1} = 250 ms. We can observe that for both the MC and SC approaches the network throughput increases as the number of mmAPs grows. The MC cases (with and without CoMP) provide always a higher network throughput with respect to the SC

approach, which is reflected also in the average number of interruptions per UE. Indeed, for $M = 5$ and $U = 20$ the number of time slots without any active links per UE is equal to 6 and 9 for the MC and SC cases, respectively. The gap between these latter at $M = 1$ is due to the fact that even with only one mmAP, MC can rely on the support of the 5G-LB, which allows the links to be prepared in advance, even in NLOS.

In Fig. 3, the difference between the solution of Algorithm 1 and MC without CoMP is very small. For this reason, we can conclude that most of the gain of Algorithm 1 with respect to the SC approach is given by the multiple connections, the fast link switching and the 5G-LB support. In this case, the improvement in terms of network throughput given by using CoMP transmissions is relatively small, which means that it is more efficient to serve more UEs with different links than to serve a lower amount of UEs by providing them multiple transmitting links. This is due to the relation between the active links and the UE's rate in the CoMP case, which is given by (2). Moreover, given P_{tot}, P_a, and P_h, the maximum number of A and H links per time slot per mmAP is 4 and the number of UEs is $U = 20$. Therefore, for most of the cases in Fig. 3, the number of LOS links is lower than the number of UEs and the NC does not take advantages from CoMP.

Indeed, when we increase the maximum number of transmitting links per mmAP per time slot, i.e. P_{tot}, the difference between the MC without and with CoMP transmissions increases in favor of the latter. This is shown in Fig. 4. Moreover, we can observe that, when the number of available links goes above a certain threshold, the slope of the curves decreases and, for any of the considered schemes, increasing P_{tot} becomes less beneficial. This phenomenon (though less evident) appears also in Fig. 3, where the number of available links indirectly increases by increasing the number of mmAPs. Finally, Fig. 5 shows the comparison among the different approaches when varying the inter-arrival link interruptions rate λ with a fixed number of UEs $U = 20$ and mmAPs $M = 5$. We observe that the gap between SC and MC cases decreases with λ (i.e. when λ^{-1} increases). As a matter of fact, when the interruptions become less frequent, the links are more stable and, therefore, the advantages of fast link switching are less evident.

VI. Conclusion

We have considered optimal link scheduling in an multi-connectivity mm-wave cellular network with the objective of maximizing the network throughput over a certain time window with constrained total power budget per mmAP. The proposed column generation approach in

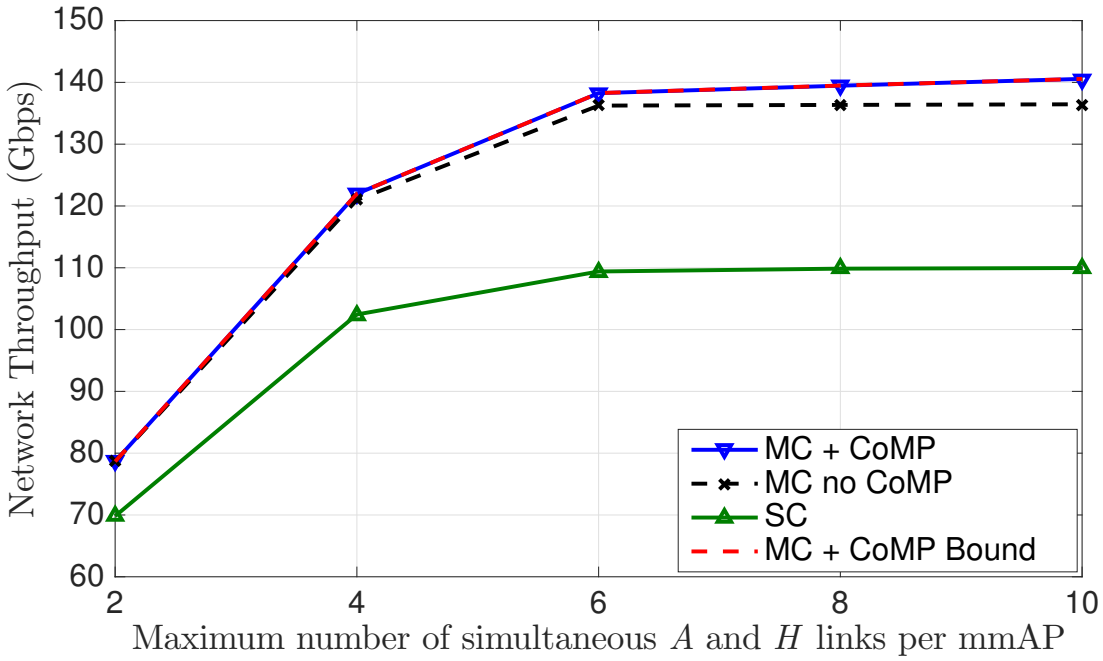

Fig. 4: Network throughput when varying the total power budget expressed in terms of maximum number of simultaneous A and H links, for $M = 5$ and $U = 30$ and λ^{-1} = 250 ms.

Algorithm 1 leads to a solution that is very close or even equal to the global optimum. Numerical results show the potential gain of multi-connectivity in millimeter-wave cellular networks. The proposed solution results in significant improvement of the network throughput with respect to the SC case. The improvement is more profound when the number of mmAPs increases or the link interruptions are more frequent.

Extensions of this work include investigating the benefits of multi-connectivity when minimizing the number of interruptions and considering error-prone prediction of the channel quality information exploited by the network controller.

ACKNOWLEDGMENT

The authors would like to thank Dr. Danish Aziz, Dr. Paolo Baracca, Dr. Lutz Ewe and Dr. Vangelis Angelakis for the insightful discussions. This work has received funding from the European Union's Horizon 2020 research and innovation programme under the Marie Sklodowska-Curie grant agreement No. 643002. Furthermore, this work has been partially supported by CENIIT.

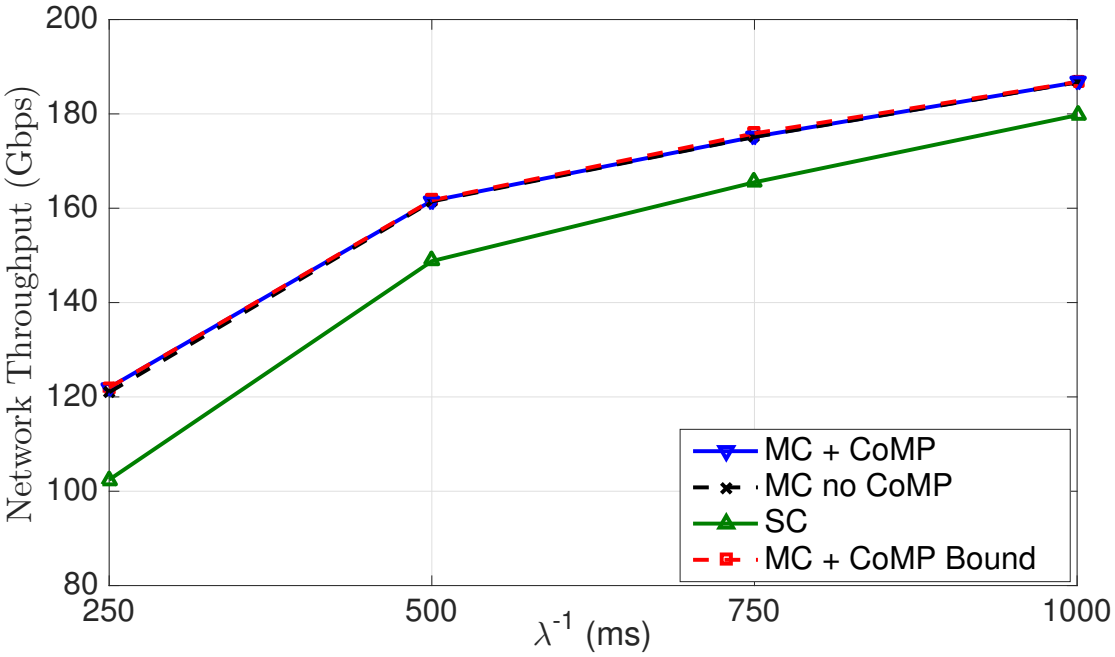

Fig. 5: Network throughput when varying the interruption parameter λ, for $M = 5$ and $U = 30$.

REFERENCES

[1] NGMN Alliance, "5G white paper," Tech. Rep., Mar. 2015.

[2] J. Choi, "On the macro diversity with multiple bss to mitigate blockage in millimeter-wave communications," *IEEE Communications Letters*, vol. 18, no. 9, pp. 1653–1656, Sept. 2014.

[3] V. Petrov, D. Solomitckii, A. Samuylov, M. A. Lema, M. Gapeyenko, D. Moltchanov, S. Andreev, V. Naumov, K. Samouylov, M. Dohler, and Y. Koucheryavy, "Dynamic multi-connectivity performance in ultra-dense urban mmwave deployments," *IEEE Journal on Selected Areas in Communications*, vol. 35, no. 9, pp. 2038–2055, Sept. 2017.

[4] D. Aziz, J. Gebert, A. Ambrosy, H. Bakker, and H. Halbauer, "Architecture approaches for 5G millimetre wave access assisted by 5G low-band using multi-connectivity," in *IEEE Globecom Workshops (GC Wkshps)*, Dec. 2016, pp. 1–6.

[5] M. Giordani, M. Mezzavilla, S. Rangan, and M. Zorzi, "Multi-connectivity in 5G mmwave cellular networks," in *Mediterranean Ad Hoc Networking Workshop (Med-Hoc-Net)*, Jun. 2016, pp. 1–7.

[6] L. Cheng, M. M. U. Gul, F. Lu, M. Zhu, J. Wang, M. Xu, X. Ma, and G. K. Chang, "Coordinated multipoint transmissions in millimeter-wave radio-over-fiber systems," *Journal of Lightwave Technology*, vol. 34, no. 2, pp. 653–660, Jan. 2016.

[7] H. Shokri-Ghadikolaei and C. Fischione, "The transitional behavior of interference in millimeter wave networks and its impact on medium access control," *IEEE Transactions on Communications*, vol. 64, no. 2, pp. 723–740, Feb. 2016.

[8] 3GPP, "Evolved universal terrestrial radio access network (e-utran); architecture description (release 14), 3GPP TS 36.401 V14.0.0," Tech. Rep., Nov. 2017.

[9] M. Giordani, M. Mezzavilla, and M. Zorzi, "Initial access in 5G mmwave cellular networks," *IEEE Communications Magazine*, vol. 54, no. 11, pp. 40–47, Nov. 2016.

[10] L. Lei, D. Yuan, C. K. Ho, and S. Sun, "Optimal cell clustering and activation for energy saving in load-coupled wireless networks," *IEEE Transactions on Wireless Communications*, vol. 14, no. 11, pp. 6150–6163, Nov. 2015.

[11] M. Gapeyenko, A. Samuylov, M. Gerasimenko, D. Moltchanov, S. Singh, M. R. Akdeniz, E. Aryafar, N. Himayat, S. Andreev, and Y. Koucheryavy, "On the temporal effects of mobile blockers in urban millimeter-wave cellular scenarios," *IEEE Transactions on Vehicular Technology*, vol. 66, no. 11, pp. 10 124–10 138, Nov. 2017.

[12] 3GPP, "Study on channel model for frequencies from 0.5 to 100 GHz (release 14), 3GPP TR 38.901 V14.2.0," Tech. Rep., Sept. 2017.

Throughput Analysis for Relay-Assisted Millimeter-Wave Wireless Networks

Cristian Tatino*†, Nikolaos Pappas*, Ilaria Malanchini†, Lutz Ewe†, Di Yuan*

*Department of Science and Technology, Linköping University, Sweden

Email: {cristian.tatino, nikolaos.pappas, di.yuan}@liu.se †Nokia Bell Labs, Stuttgart, Germany

Email: {ilaria.malanchini, lutz.ewe}@nokia-bell-labs.com

Abstract

In this work, we analyze the throughput of random access multi-user relay-assisted millimeter-wave wireless networks, in which both the destination and the relay have multi-packet reception capability. We consider a full-duplex network cooperative relay that stores the successfully received packets in a queue, for which we analyze the performance. Moreover, we study the effects on the network throughput of two different schemes, by which the source nodes transmit either a packet to both the destination and the relay in the same timeslot by using wider beams (broadcast scheme) or to only one of these two by using narrower beams (fully directional scheme). Numerical results show how the network throughput varies according to specific system parameters, such as positions and number of nodes. The analysis allows us also to understand the optimal transmission scheme for different network scenarios and shows that the choice to use transmissions with narrow beams does not always represent the best strategy, as wider beams provide a lower beamforming gain, but they allow to transmit simultaneously both at the relay and the destination.

I. Introduction

Given the exponential growth of data rate and connections for the fifth generation (5G) of wireless networks, millimeter-wave (mm-wave) communications technology has attracted the interest of many researchers in the past few years. The abundance of spectrum resource in the

This project has received funding from the European Union's Horizon 2020 research and innovation programme under the Marie Sklodowska-Curie grant agreement No. 643002.

mm-wave frequency range (30-300 GHz) could help to deal with the longstanding problem of spectrum scarcity. However, the signal propagation in the mm-wave frequency range is subject to more challenging conditions in comparison to lower frequency communications, especially in terms of path loss and penetration loss, which causes frequent communication interruptions.

Several solutions have been proposed in order to overcome the blockage issue, e.g., cell densification, multi-connectivity and relaying techniques. Although relay has been extensively investigated for microwave frequencies [1]–[5], mm-wave communications present peculiarities that make further analysis necessary. As an example, in contrast to broadcast transmissions (mainly used for lower frequency bands), mm-waves use narrow beams with higher beamforming gain to overcome the path loss issue. By using these transmissions (fully directional scheme, FD), a source node (user equipment, UE) sends a packet either to the relay or to the destination (mm-wave access point, mmAP). On the other hand, in the broadcast communication case (BR), a packet that is sent by a UE can be received by both the relay and the mmAP in the same timeslot.

In this work, we analyze the throughput of network cooperative communications in a multi-user mm-wave wireless network. We evaluate two types of transmissions, i.e., FD and BR. When the UEs use a BR scheme and the transmission to the destination fails, the relay stores the packets (that are correctly decoded) in its queue and is responsible to transmit it to the destination. This technique is also known as network level cooperation relaying [2]–[5].

A. Related Work

The benefits of relaying techniques for mm-wave wireless networks have been discussed in several works, e.g, [6]–[12]. In [6] and [7], stochastic geometry is used to analyze the system performance for a relay-assisted mm-wave cellular network. Authors analyze several relay selection techniques and they show a significant improvement in terms of signal-to-interference-plus-noise ratio (SINR) distribution and coverage probability. In [8], authors propose a two-hop relay selection algorithm for mm-wave communications that takes into account the dependency between the source-destination and relay-destination paths in terms of line-of-sight (LOS) probability. In [9], a joint relay selection and mmAP association problem is considered. In particular, the authors propose a distributed solution that takes into account the load balancing and fairness aspects among multiple mmAPs. Other works, [10] and [11], focus on relaying

techniques for device-to-device (D2D) scenarios and analyze, by using stochastic geometry, the coverage probability and the relay selection problem, respectively.

The authors of [12] analyze the tradeoff between mm-wave relay and microwave frequency transmissions for a two-hop half-duplex relay scenario. They study the throughput and delay for a single source-destination pair and a single relay, which can transmit on mm-wave frequencies or by using microwave frequencies when the direct path is blocked. To the best of our knowledge, the setup considered in this paper has been investigated only for microwave frequencies [4], without taking into account different transmission strategies.

B. Contributions

In this work, we provide an analysis of the throughput for random access multi-user cooperative relaying mm-wave wireless networks. We consider two different transmission schemes, i.e., FD and BR that may provide different beamforming gains and cause different interference levels. Indeed, BR transmissions may provide a lower beamforming gain with respect to the FD scheme, but they allow to transmit simultaneously both at the relay and the mmAP. The UEs, independently, choose to transmit by following one of the schemes and we identify the optimal strategy with respect to system parameters; namely, we show under which conditions BR transmissions should be preferred to a FD scheme and vice-versa. Furthermore, by using queueing theory, we study the performance characteristic of the queue at the relay, for which we derive the stability condition, as well as the service and the arrival rate.

The rest of the paper is organized as follows: in Section II, we describe the system model and the assumptions. In Section III, we present the queue analysis at the relay with two UEs and in Section IV, we generalize these results and evaluate the aggregate network throughput for N UEs. In Section V, we illustrate the results and performance evaluation and Section VI concludes the paper.

II. System Model and Assumptions

A. Network Model

We consider a set of symmetric[1] UEs $\mathcal{N}$, with cardinality N. We consider one mmAP (destination) and one full-duplex relay (R) that operates in a decode-forward manner. We assume

[1]Symmetric UEs have the same mm-wave networking characteristics, e.g., propagation conditions. Our study can be generalized to the asymmetric case; however, the analysis will be dramatically involved without providing any additional meaningful insights.

multiple packet reception capability both at the mmAP and the R which are equipped with hybrid beamformers and they can form multiple beams at the same time [13]. The UEs are equipped with analog beamformers, which can form one beam at a time. We assume slotted time and each packet transmission takes one timeslot. The relay has no packets of its own, but it stores the successfully received packets from the UEs in a queue, which has infinite size[2] and bursty arriving traffic. The UEs have saturated queues, i.e, they are never empty. We assume that acknowledgments (ACKs) are instantaneous and error free and packets received successfully are deleted from the queues of the transmitting nodes, i.e., UEs and R.

UEs and R transmit a packet with probabilities q_u and q_r, respectively. As mentioned previously, a UE can transmit by using either the FD or the BR scheme with probabilities q_{uf} and q_{ub} ($q_{uf} = 1 - q_{ub}$), which are conditioned to the event that a packet is transmitted. In turn, when a UE uses the FD transmission, it transmits either to the mmAP or to R with probabilities q_{ud} and q_{ur} ($q_{ud} = 1 - q_{ur}$), respectively, which are conditioned probabilities to the event that a packet is transmitted by using the FD scheme. In the BR case, R stores the successfully received packets only when these are not received by the mmAP and the relay always uses directional communications to forward them to the mmAP. In Fig. 1, we illustrate an example of the FD and BR transmissions, where d_{ur} and d_{ud} represent the distances between the UE and R and between the UE and the mmAP, respectively. The parameter θ_{rd} is the angle formed by R and the mmAP with a UE as vertex and θ_{BW} is the beamwidth. Hereafter, we indicate the probability of the complementary event by a bar over the term (e.g., $\overline{q}_u = 1 - q_u$). Moreover, we use superscripts f and b to indicate the FD and BR transmissions, respectively.

B. SINR Expression and Success Probability

A packet is successfully received if the SINR is above a certain threshold γ. Ideally, multiple transmissions at the receiver side of a node do not interfere when they are received on different beams. However, in real scenarios, interference cancellation techniques are not perfect; thus, we introduce a coefficient $0 \leq \alpha \leq 1$ that models the interference between received beams. The cases $\alpha = 0$ and $\alpha = 1$ represent perfect interference cancellation and no interference cancellation, respectively. In order to keep the clarity of the presentation we consider α constant. Moreover, we assume that an FD transmission to the mmAP does not interfere with the packet transmitted

[2]A similar analysis can be derived for the case of finite queue size, which will be treated in an extension of this work.

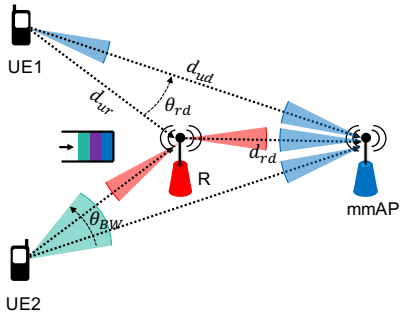

Fig. 1: FD (UE1) and BR (UE2) transmissions in a scenario with two UEs, one relay and one mmAP. In this example, UE1 is transmitting to the mmAP.

to R and vice-versa. On the other hand, when a UE uses a BR scheme, its transmission interferes with the transmissions of the other UEs for both the mmAP and R.

$$\begin{aligned}&\text{SINR}^{f}_{ij/\mathcal{I}_{fl},\mathcal{I}_{fn},\mathcal{I}_{bl},\mathcal{I}_{bn}}|\text{LOS}_{ij}\\&=\frac{p_t g_i^f g_j^f h_l(i,j)}{p_N+\alpha\Big(\sum\limits_{k\in\mathcal{I}_{fl}} p^f_{r/l}(k,j)+\sum\limits_{m\in\mathcal{I}_{bl}} p^b_{r/l}(m,j)+\sum\limits_{u\in\mathcal{I}_{fn}} p^f_{r/n}(u,j)+\sum\limits_{v\in\mathcal{I}_{bn}} p^b_{r/n}(v,j)\Big)}.\end{aligned} \tag{1}$$

We assume that the links between all pairs of nodes are independent and can be in two different states, LOS and non-line-of-sight (NLOS). Specifically, LOS_{ij} and NLOS_{ij} are the events that node i is in LOS and NLOS with node j, with associated probabilities $P(\text{LOS}_{ij})$ and $P(\text{NLOS}_{ij})$, respectively. Furthermore, we assume that R is placed in a position that guarantees the LOS with the mmAP, namely, $P(\text{LOS}_{rd}) = 1$. In order to compute the SINR for link ij, we first identify the sets of interferers that use FD and BR transmissions, which are $\mathcal{I}_f$ and $\mathcal{I}_b$, respectively. Then, we partition each of them into the sets of nodes that are in LOS and NLOS with node j. These sets are $\mathcal{I}_{fl}$ and $\mathcal{I}_{fn}$, for the nodes that use the FD scheme and $\mathcal{I}_{bl}$ and $\mathcal{I}_{bn}$ for the UEs that use the BR transmissions. Therefore, when node i is in LOS with node j, we can write the SINR, conditioned to $\mathcal{I}_{fl}, \mathcal{I}_{fn}, \mathcal{I}_{bl}, \mathcal{I}_{bn}$, as in (1).

The beamforming gain of the transmitter and the receiver are g_i and g_j, respectively. These are computed in according to the ideal sectored antenna model [14], which is given by: $g_i = g_j = \frac{2\pi}{\theta_{BW}}$ in the main lobe, and 0 otherwise. The term $h_l(i,j)$ is the path loss on link ij when this is in LOS. The transmit and the noise power are p_t and p_N, respectively. The terms $p_{r/l}(i,j)$ and $p_{r/n}(i,j)$ represent the received power by node j from node i, when the first is in LOS and NLOS, respectively. Note that similar expressions of the SINR can be derived also in case

of BR and NLOS. Finally, the success probabilities for a packet sent on link ij by using FD and BR transmissions are represented by the terms $P^f_{ij/\mathcal{I}_f,\mathcal{I}_b}$ and $P^b_{ij/\mathcal{I}_f,\mathcal{I}_b}$, respectively. Here, we consider only the conditioning on the sets $\mathcal{I}_f$ and $\mathcal{I}_b$, since we average over all possible scenarios for the LOS and NLOS link conditions. The expression for the FD transmission and N UEs is given in Appendix A.

III. Performance Analysis for the Relay Queue

In order to compute the network throughput, in this section, we evaluate the arrival rate, λ, for the queue at R, for which we further analyze the service rate, μ_r, and the stability condition. Namely, we present the results for two UEs to give insights to understand the throughput analysis, which is generalized for N UEs in Section IV. First, similar to [4], we compute λ as follows:

$$\lambda = P(Q=0)\lambda_0 + P(Q\neq 0)\lambda_1, \tag{2}$$

where λ_0 and λ_1 are the arrival rates at R when the queue is empty or not, which occur with probabilities $P(Q=0)$ and $P(Q\neq 0)$, respectively. Namely, when the queue is not empty, R may transmit and interfere with the other transmissions to the mmAP. Therefore, by considering all the possible combinations for the two UEs scenario, where R can receive at maximum two packets per timeslot, we can compute λ_0 and λ_1. Note that the definition of the sets $\mathcal{I}_f$ and $\mathcal{I}_b$ can be simplified since the UEs are symmetric. Therefore, it is sufficient to indicate the number of UEs that are interfering and whether R is transmitting, i.e., we indicate with $\{|\mathcal{I}_f|, r\}^f$ and $\{|\mathcal{I}_f|\}^f$ the sets of interferers that use FD transmissions when R is transmitting or not, respectively, and with $\{r\}^f$ the set of interferers when only the relay is transmitting. Therefore, we obtain:

$$\begin{aligned}
\lambda_0 &= 2q_u\overline{q}_u q_{uf} q_{ur} P^f_{ur} + 2q_u\overline{q}_u q_{ub} P^b_{ur}\overline{P}^b_{ud} \\
&+ q_u^2 q_{uf}^2 q_{ur}^2 q_{ur}^2 \Big[2P^f_{ur/\{1\}^f}\overline{P}^f_{ur/\{1\}^f} \\
&+ 2\Big(P^f_{ur/\{1\}^f}\Big)^2\Big] + 2q_u^2 q_{uf}^2 q_{ur} q_{ud} P^f_{ur} \\
&+ 2q_u^2 q_{1f} q_{ub} q_{ur}\Big[P^f_{ur/\{1\}^b}\Big(1 - P^b_{ur/\{1\}^f}\overline{P}^b_{ud}\Big) \\
&+ \overline{P}^f_{ur/\{1\}^b} P^b_{ur/\{1\}^f}\overline{P}^b_{ud} + 2\Big(P^b_{ur/\{1\}^f}\overline{P}^b_{ud}\Big)^2\Big] \\
&+ 2q_u^2 q_{ub} q_{uf} q_{ud} P^b_{ur}\overline{P}^b_{ud/\{1\}^f} \\
&+ q_u^2 q_{ub}^2\Big[2P^b_{ur/\{1\}^b}\overline{P}^b_{ud/\{2\}^b}\Big(1 - P^b_{ur/\{1\}^b}\overline{P}^b_{ud/\{1\}^b}\Big)
\end{aligned}$$

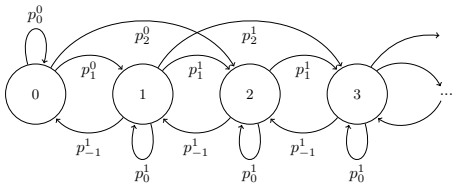

Fig. 2: The DTMC model for the two UEs case.

$$+ 2\Big(P^b_{ur/\{1\}^b}\overline{P}^b_{ud/\{1\}^b}\Big)^2\Big], \tag{3}$$

where, q_u, q_{ub}, q_{uf}, q_{ud}, and q_{ur} are introduced in Section II-A. Similarly, we obtain that $\lambda_1 = \overline{q}_r\lambda_0 + q_r A_r$, whereas the service rate is $\mu_r = q_r B_r$. The terms A_r and B_r are given in Appendix B. Now, we derive the condition for the queue stability, which is used to determine the throughput. By applying the Loyne's criterion [15], we can obtain the range of values of q_r for which the queue is stable by solving the equation $\lambda_1 = \mu_r$. Thus, we have that the queue at R is stable if and only if $q_{r_{min}} < q_r \leq 1$, where $q_{r_{min}}$ is given by:

$$q_{r_{min}} = \frac{\lambda_0}{\lambda_0 + B_r - A_r}. \tag{4}$$

The evolution of the queue at the relay can be modelled as a discrete time Markov Chain (DTMC), as reported in Fig. 2. The terms p_k^0 and p_k^1 are the probabilities that the queue size increases by k packets, in a timeslot, when the queue is empty or not, respectively, and their expressions are reported in Appendix C. Finally, by omitting the details for sake of space, we compute $P(Q = 0)$ by considering the Z-transformation of the steady-state distribution vector [16]:

$$P(Q = 0) = \frac{p_{-1}^1 - p_1^1 - 2p_2^1}{p_{-1}^1 - p_1^1 - 2p_2^1 + \lambda_0}. \tag{5}$$

IV. Throughput Analysis

In this section, we derive the network aggregate throughput, T, for N UEs by generalizing the results obtained in Section III. In particular, we distinguish between two cases. First, when the queue is stable, T is given by:

$$T = NT_u = N(T_{ud} + T_{ur}), \tag{6}$$

where T_u represents the per-user throughput. This is composed by two terms, T_{ud} and T_{ur}, which represent the contributions to T_u given by the packets received by the mmAP or by R, respectively. Second, when the queue at R is unstable, the aggregate throughout is:

$$T = NT_{ud} + \mu_r. \tag{7}$$

In particular, the expressions for T_{ud} and T_{ur} can be derived as follows. We indicate with m the number of UEs that interfere and with i the number of those that use FD transmissions ($m - i$ UEs use the BR scheme). A certain number, j, of FD interferers transmit to R and $i - j$ to the mmAP. Therefore, T_{ud} and T_{ur} are given by:

$$T_{ud} = \Big(1 - q_r P(Q \neq 0)\Big) T^0_{ud} + q_r P(Q \neq 0) T^1_{ud}, \tag{8}$$

$$\begin{aligned} T_{ur} = {} & q_u q_{uf} q_{ur} \sum_{m=0}^{N-1} \binom{N-1}{m} q_u^m \overline{q}_u^{N-1-m} \\ & \times \sum_{i=0}^{m} \binom{m}{i} q_{uf}^i q_{ub}^{m-i} \sum_{j=0}^{i} \binom{i}{j} q_{ur}^j q_{ud}^{i-j} \\ & \times P^f_{ur/\{j\}^f,\{m-i\}^b} + \Big(1 - q_r P(Q \neq 0)\Big) T^0_{ur} \\ & + q_r P(Q \neq 0) T^1_{ur}, \end{aligned} \tag{9}$$

where $P(Q = 0)$, derived by following the same method used in Section III, but for N UEs, is given by:

$$P(Q = 0) = \frac{p^1_{-1} - \sum_{k=1}^{N} k p^1_k}{p^1_{-1} - \sum_{k=1}^{N} k p^1_k + \lambda_0}. \tag{10}$$

In this case, p^1_k, p^1_{-1} and λ_0 have the same meaning as for the two UEs case, but different values. The terms T^0_{ud} and T^1_{ud} represent the contribution to T_u given by the packets sent to the mmAP (when R is interfering or not) and are given by:

$$\begin{aligned} T^0_{ud} = {} & q_u q_{uf} q_{ud} \sum_{m=0}^{N-1} \binom{N-1}{m} q_u^m \overline{q}_u^{N-1-m} \sum_{i=0}^{m} \binom{m}{i} q_{uf}^i q_{ub}^{m-i} \\ & \times \sum_{j=0}^{i} \binom{i}{j} q_{ur}^j q_{ud}^{i-j} P^f_{ud/\{i-j\}^f,\{m-i\}^b} \\ & + q_u q_{ub} \sum_{m=0}^{N-1} \binom{N-1}{m} q_u^m \overline{q}_u^{N-1-m} \sum_{i=0}^{m} \binom{m}{i} q_{uf}^i q_{ub}^{m-i} \\ & \times \sum_{j=0}^{i} \binom{i}{j} q_{ur}^j q_{ud}^{i-j} \times P^b_{ud/\{i-j\}^f,\{m-i\}^b}, \end{aligned} \tag{11}$$

$$T_{ud}^{1} = q_u q_{uf} q_{ud} \sum_{m=0}^{N-1} \binom{N-1}{m} q_u^m \overline{q}_u^{N-1-m} \sum_{i=0}^{m} \binom{m}{i} q_{uf}^i q_{ub}^{m-i} \times \sum_{j=0}^{i} \binom{i}{j} q_{ur}^j q_{ud}^{i-j} P^f_{ud/\{i-j,r\}^f,\{m-i\}^b} + q_u q_{ub} \sum_{m=0}^{N-1} \binom{N-1}{m} q_u^m \overline{q}_u^{N-1-m} \sum_{i=0}^{m} \binom{m}{i} q_{uf}^i q_{ub}^{m-i} \times \sum_{j=0}^{i} \binom{i}{j} q_{ur}^j q_{ud}^{i-j} P^b_{ud/\{i-j,r\}^f,\{m-i\}^b}. \quad (12)$$

Finally, we derive the terms T_{ur}^0 and T_{ur}^1:

$$T_{ur}^{0} = q_u q_{ub} \sum_{m=0}^{N-1} \binom{N-1}{m} q_u^m \overline{q}_u^{N-1-m} \times \sum_{i=0}^{m} \binom{m}{i} q_{uf}^i q_{ub}^{m-i} \sum_{j=0}^{i} \binom{i}{j} q_{ur}^j q_{ud}^{i-j} \times P^b_{ur/\{j\}^f,\{m-i\}^b} \overline{P}^b_{ud/\{i-j\}^f,\{m-i\}^b}. \quad (13)$$

$$T_{ur}^{1} = q_u q_{ub} \sum_{m=0}^{N-1} \binom{N-1}{m} q_u^m \overline{q}_u^{N-1-m} \times \sum_{i=0}^{m} \binom{m}{i} q_{uf}^i q_{ub}^{m-i} \sum_{i=0}^{i} \binom{i}{j} q_{ur}^j q_{ud}^{i-j} \times P^b_{ur/\{j\}^f,\{m-i\}^b} \overline{P}^b_{ud/\{i-j,r\}^f,\{m-i\}^b}. \quad (14)$$

V. Numerical Results

In this section, we provide the numerical evaluation of the analysis derived in the previous sections. In order to compute the LOS and NLOS probabilities and the path loss, we use the 3GPP model for urban micro cells in outdoor street canyon environment [17]. More precisely, the path loss depends on the height of the mmAP, 10 m, the height of the UE, 1.5 m, the carrier frequency, $f_c = 30$ GHz and the distance between the transmitter and the receiver. The transmit and the noise power are set to $P_t = 24$ dBm and $P_N = -80$ dBm, respectively. Then, the SINR in (1) and the success probability in (15) are numerically computed.

Hereafter, we show the network throughput (T) while varying several parameters. Unless otherwise specified, we set $d_{ur} = 30$ m, $d_{ud} = 50$ m, $\gamma = 10$ dB and $\alpha = 0.1$. Moreover, we set either $\theta_{BW} = 5^\circ$ or $\theta_{BW} = \theta_{rd}$ for the FD and BR transmissions, respectively. In Fig. 3, we

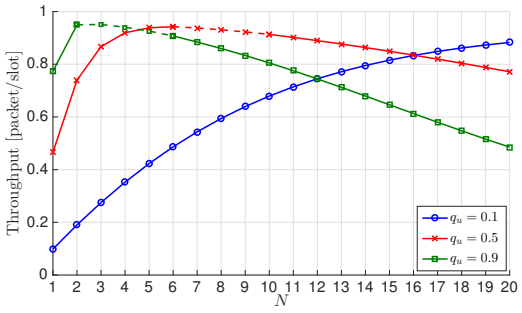

Fig. 3: T while varying N for several values of q_u, with $\theta_{rd} = 30°$ and $q_{ur} = 0.5$. Solid and dotted lines are used for the range of UEs where the queue is stable or unstable, respectively.

show T while varying the number of UEs for several UE transmit probability values, i.e., q_u. In particular, we use solid lines when the queue at R is stable (cf. Eq. (6)) and the dotted lines when the queue is unstable (cf. Eq. (7)). For $q_u = 0.1$ the queue is always stable, in contrast, for $q_u = 0.5$ and $q_u = 0.9$ the queue becomes unstable at $N = 7$ and $N = 3$, respectively. Above a certain number of UEs, T reaches almost the maximum value and then it start decreasing. Namely, for $q_u = 0.5$ and $q_u = 0.9$, the queue becomes again stable at $N = 10$ and $N = 6$, respectively, because high values of N and q_u lead to high interference that decreases the number of packets successfully received by R and the mmAP.

In Fig. 4, we show the T while varying the probability of using the FD scheme, q_{uf}, and θ_{rd}. Hereafter, we set $q_u = 0.1$ and $N = 10$ and we can observe that the optimal choice of q_{uf} depends on θ_{rd}. Namely, for small values of θ_{rd}, BR transmissions are more preferable, which correspond to small values of q_{uf}. Indeed, in this case, we can use beams with high beamforming gain to transmit simultaneously to R and the mmAP. In contrast, for higher values of θ_{rd}, the optimal value of q_{uf} is 1 that corresponds to always use the FD scheme. Furthermore, it is possible to observe that for $q_{uf} = 1$, T increases with θ_{rd}. This is caused by the interference of R on the communications between the UEs and the mmAP.

This phenomenon can be better observed in Fig. 5, which shows both the aggregate throughput received by the mmAP and by R, i.e., T_d and T_r, for several values of q_{uf} while varying θ_{rd}. Larger values of θ_{rd} correspond to longer distances between R and the mmAP, i.e., d_{rd}. For $q_{uf} = 1$, the success probability for a packet transmitted from R to the mmAP, and so T_r (dotted lines), are barely affected by increasing the link length. Indeed, the link R-mmAP is always in LOS. In contrast T_d (solid lines) increases for wider θ_{rd} because the interference caused by R

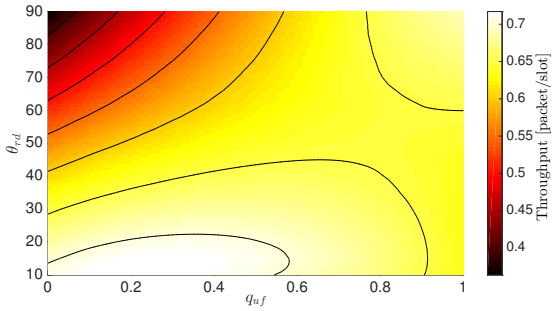

Fig. 4: T while varying q_{uf} and θ_{rd} for $N = 10$ and $q_{ur} = 0.5$.

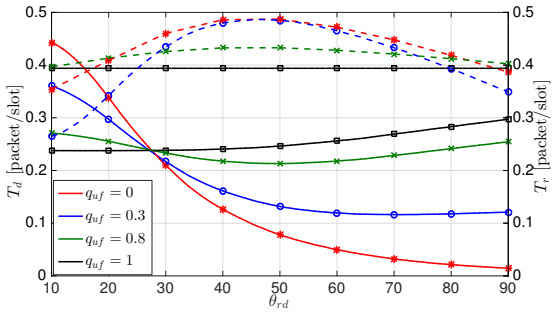

Fig. 5: T_d (solid lines) and T_r (dotted lines) with varying θ_{rd} for several values of q_{uf} and $q_{ur} = 0.5$.

decreases. For $0 < q_{uf} < 1$, T_d and T_r have a non-monotonic behavior. Initially, as θ_{rd} increases, T_d decreases because of two reasons. First, the beamforming gain of the BR transmissions decreases, and so the success probability for a packet sent by using the BR scheme. Second, since the packets that are not successfully received by the mmAP may increase the number of packets in the queue at R, both T_r and the interference at the receiver side of the mmAP (caused by the relay) also increase. However, above a certain value of θ_{rd}, T_r starts decreasing because wider beams with lower beamforming gains are not enough to overcome the path loss. Fig. 6 shows similar results of Fig. 4, but with a higher SINR threshold, i.e., $\gamma = 20$ dB. In this case, we can observe that the best transmission strategy is always the FD scheme, even for low value of θ_{rd}. The reason behind is that the beamforming gain provided by the BR scheme leads to low success probabilities with respect to the FD transmission.

To give further insights into the FD scheme, we fix $q_{uf} = 1$, i.e., UEs always use the FD scheme, and increase the distances, i.e., $d_{ur} = 50$ m and $d_{ud} = 200$ m. In Fig. 7, we show T when vary θ_{rd} and q_{ur}, which is the probability to transmit to the relay. In contrast to the

previous case (Fig. 4 and Fig. 6), T decreases as θ_{rd} increases. Indeed, as d_{rd} increases, the high link path loss between R and the mmAP reduces the success probability for a packet sent from R to the mmAP. This has mainly two effects: i) it decreases the interference of R on the communications between the UEs and the mmAP and ii) it reduces the relay's service rate μ_r, which makes the queue at R not stable when q_{ur} is above certain values (which is $q_{ur} = 0.3$ for $\theta_{rd} = 30^\circ$ and decreases as θ_{rd} increases). Furthermore, we can also observe that for low values of d_{rd}, hence θ_{rd}, the highest throughput is given by $q_{ur} = 1$, whereas increasing the value of d_{rd}, hence θ_{rd}, it is better to always send packets to the relay, i.e., $q_{ur} = 0$.

Finally, in Fig. 8 we show T while varying q_{uf} for several values of d_{ur} and d_{ud}, when $\theta_{rd} = 30^\circ$. It is possible to observe that for short distances (blue curve), the optimal value of q_{uf} is smaller than 0.5. Indeed due to the small path loss values of the links UE-mmAP and UE-R, it is always favorable to use the BR scheme. In contrast, when the distances increase, the transmissions need higher beamforming gain and therefore the FD scheme is preferable.

VI. Conclusion

In this work, we have presented a throughput analysis for relay assisted mm-wave wireless networks, where the UEs can transmit by using either a FD or a BR transmission. In particular, we have evaluated the performance of the queue at the relay by deriving the stability conditions as well as the arrival and service rates. The numerical evaluation shows that the interference caused by the relay and the link path loss represent the main impediments for the success probability, hence the throughput, in case of short and long distances among the nodes, respectively. Furthermore, results show that the optimal transmission strategy (values of q_{uf} and q_{ur}) highly depends on the network topology, e.g., d_{ud}, d_{ur} and θ_{rd}.

As expected, it is not always beneficial to use narrow beams (FD) compared to wider beams (BR). As a matter of fact, for short distances and beamwidth of 30°, a BR transmission is preferable, although it provides a lower beamforming gain. When the distances or the SINR threshold increase, then the FD scheme should be chosen. Future work will investigate the behavior of the throughput as well as of the delay when taking additional aspects into account, such as the inter-beam interference cancellation technique and the beamforming alignment phase.

Appendix A

Here, we report the expression for the success probability for the link ij with N symmetric UEs, conditioned to the sets $\mathcal{I}_f$ and $\mathcal{I}_b$. We average over all the possible scenarios for the LOS

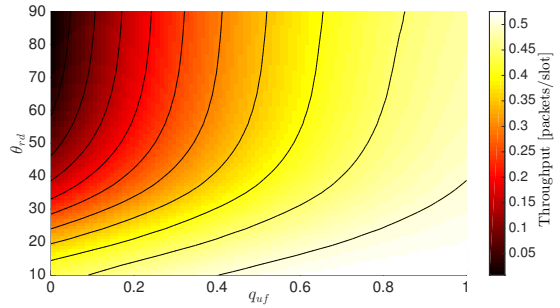

Fig. 6: T while varying q_{uf} and θ_{rd} for $N = 10$, $q_{ur} = 0.5$ and $\gamma = 20$ dB.

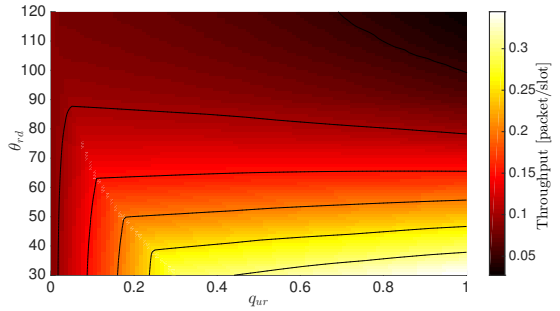

Fig. 7: T while varying θ_{rd} and q_{ur} for $q_{uf} = 1$, d_{ur}= 50 m and $d_{ud} = 200$ m.

and NLOS links. We consider that k and h UEs over $|\mathcal{I}_f|$ and $|\mathcal{I}_b|$ interferers, respectively, are in LOS. Thus, the success probability is as follows:

$$
\begin{aligned}
P^f_{ij/\mathcal{I}_f,\mathcal{I}_b} &= P(\text{LOS}_{ij})P(\text{SINR}^f_{ij/\mathcal{I}_f,\mathcal{I}_b} \geq \gamma|\text{LOS}_{ij}) \\
&+ P(\text{NLOS}_{ij})P(\text{SINR}^f_{ij/\mathcal{I}_f,\mathcal{I}_b} \geq \gamma|\text{NLOS}_{ij}) \\
&= P(\text{LOS}_{ij})\Bigg[\sum_{k=0}^{|\mathcal{I}_f|}\binom{|\mathcal{I}_f|}{k}P(\text{LOS}_{ij})^k P(\text{NLOS}_{ij})^{|\mathcal{I}_f|-k} \\
&\times \sum_{h=0}^{|\mathcal{I}_b|}\binom{|\mathcal{I}_b|}{h}P(\text{LOS}_{ij})^h P(\text{NLOS}_{ij})^{|\mathcal{I}_b|-h} \\
&\times P(\text{SINR}^f_{ij/\mathcal{I}_{fl},\mathcal{I}_{fn},\mathcal{I}_{bl},\mathcal{I}_{bn}} \geq \gamma|\text{LOS}_{ij})\Bigg] \\
&+ P(\text{NLOS}_{ij})\Bigg[\sum_{k=0}^{|\mathcal{I}_f|}\binom{|\mathcal{I}_f|}{k}P(\text{LOS}_{ij})^k P(\text{NLOS}_{ij})^{|\mathcal{I}_f|-k} \\
&\times \sum_{h=0}^{|\mathcal{I}_b|}\binom{|\mathcal{I}_b|}{h}P(\text{LOS}_{ij})^h P(\text{NLOS}_{ij})^{|\mathcal{I}_b|-h}
\end{aligned}
\tag{15}
$$

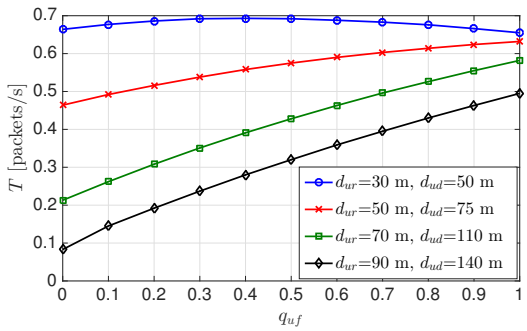

Fig. 8: T while varying q_{uf} for several values of d_{ur} and d_{ud}, when $\theta_{rd} = 30$ and $q_{ur} = 0.5$.

$$\times P(\text{SINR}^{f}_{ij/\mathcal{I}_{fl},\mathcal{I}_{fn},\mathcal{I}_{bl},\mathcal{I}_{bn}} \geq \gamma | \text{NLOS}_{ij}) \Bigg].$$

The expressions $P(\text{SINR}^{f}_{ij/\mathcal{I}_f,\mathcal{I}_b} \geq \gamma|\text{LOS}_{ij})$ and $P(\text{SINR}^{f}_{ij/\mathcal{I}_f,\mathcal{I}_b} \geq \gamma|\text{NLOS}_{ij})$ are the probabilities, conditioned to the specific scenarios of interferers, $\mathcal{I}_f$ and $\mathcal{I}_b$, that the received SINR is above γ, when link ij is in LOS and NLOS, respectively.

APPENDIX B

In this appendix, we report the terms A_r and B_r, which are used in Section III for the expressions of λ_1 and μ_r, respectively, and can be computed similarly to λ_0:

$$\begin{aligned}
A_r = {} & 2q_u\overline{q}_u q_{uf} q_{ur} P^{f}_{ur} + 2q_u\overline{q}_u q_{ub} P^{b}_{ur}\overline{P}^{b}_{ud} \\
& + q_u^2 q_{uf}^2 q_{ur}^2 q_{ur}^2 \Big[2P^{f}_{ur/\{1\}^f}\overline{P}^{f}_{ur/\{1\}^f} \\
& + 2\Big(P^{f}_{ur/\{1\}^f}\Big)^2\Big] + 2q_u^2 q_{uf}^2 q_{ur} q_{ud} P^{f}_{ur} \\
& + 2q_u^2 q_{1f} q_{ub} q_{ur} \Big[P^{f}_{ur/\{1\}^b}\Big(1 - P^{b}_{ur/\{1\}^f}\overline{P}^{b}_{ud/\{r\}^f}\Big) \\
& + \overline{P}^{f}_{ur/\{1\}^b} P^{b}_{ur/\{1\}^f}\overline{P}^{b}_{ud/\{r\}^f} + 2\Big(P^{b}_{ur/\{1\}^f}\overline{P}^{b}_{ud/\{r\}^f}\Big)^2\Big] \\
& + 2q_u^2 q_{ub} q_{uf} q_{ud} P^{b}_{ur}\overline{P}^{b}_{ud/\{1,r\}^f} + q_u^2 q_{ub}^2 \\
& \times \Big[2P^{b}_{ur/\{1\}^b}\overline{P}^{b}_{ud/\{r\}^f,\{1\}^b}\Big(1 - P^{b}_{ur/\{1\}^b}\overline{P}^{b}_{ud/\{r\}^f,\{1\}^b}\Big) \\
& + 2\Big(P^{b}_{ur/\{1\}^b}\overline{P}^{b}_{ud/\{r\}^f,\{1\}^b}\Big)^2\Big].
\end{aligned} \tag{16}$$

$$B_r = P^{f}_{rd}\Big(\overline{q}_u^2 + 2q_u\overline{q}_u q_{uf} q_{ur} + q_u^2 q_{uf}^2 q_{2f} q_{ur}^2\Big)$$

$$
\begin{aligned}
&+ P^{f}_{rd/\{1\}^{f}}\Big(2q_u\overline{q}_u q_{uf}q_{ud} + 2q_u^2 q_{uf}^2 q_{ud}q_{ur}\Big)\\
&+ P^{f}_{rd/\{1\}^{b}}\Big(2q_u\overline{q}_u q_{ub} + 2q_u^2 q_{ub}q_{uf}q_{ur}\Big)\\
&+ P^{f}_{rd/\{2\}^{f}} q_u^2 q_{uf}^2 q_{ud}^2 + P^{f}_{rd/\{1\}^{f},\{1\}^{b}} 2q_u q_{uf} q_{ub} q_{ud}\\
&+ P^{f}_{rd/\{2\}^{b}} q_u^2 q_{ub}^2.
\end{aligned} \tag{17}
$$

APPENDIX C

Hereafter, we present the transition probabilities p_k^0 and p_k^1 for the two UEs case.

$$
\begin{aligned}
p^1_{-1} = q_r\Big[&P^{f}_{rd}\Big(\overline{q}_u^2 + 2q_u\overline{q}_u q_{uf}q_{ur}\overline{P}^{f}_{ur}\\
&+ (q_u q_{uf} q_{ur}\overline{P}^{f}_{ur/\{1\}^{f}})^2\Big) + P^{f}_{rd/\{1\}^{f}}\\
&\times\Big(2q_u\overline{q}_u q_{uf}q_{ud} + 2q_1^2 q_{uf}^2 q_{ud}q_{ur}\overline{P}^{f}_{ur}\Big)\\
&+ P^{f}_{rd/\{1\}^{b}}\Big(2q_u\overline{q}_u q_{ub}(1 - P^{b}_{ur}\overline{P}^{b}_{ud/\{r\}^{f}})\\
&+ 2q_u^2 q_{ub}q_{uf}q_{ur}(1 - P^{b}_{ur/\{1\}^{f}}\overline{P}^{b}_{ud/\{r\}^{f}})\overline{P}^{f}_{ur/\{1\}^{b}}\Big)\\
&+ P^{f}_{rd/\{1\}^{f},\{1\}^{b}} 2q_u^2 q_{uf}q_{ub}q_{ud}(1 - P^{b}_{ur}\overline{P}^{b}_{ud/\{1,r\}^{f}})\\
&+ P^{f}_{rd/\{2\}^{b}}\Big(q_u q_{ub}(1 - P^{b}_{ur/\{1\}^{b}}\overline{P}^{b}_{ud/\{r\}^{f},\{1\}^{b}})\Big)^2\Big]\\
&+ P^{f}_{rd/\{2\}^{f}} q_u^2 q_{uf}^2 q_{ud}^2.
\end{aligned} \tag{18}
$$

$$
\begin{aligned}
p^0_1 = &\,2q_u\overline{q}_u q_{uf}q_{ur}P^{f}_{ur} + 2q_u\overline{q}_u q_{ub}P^{b}_{ur}\overline{P}^{b}_{ud}\\
&+ 2q_u^2 q_{uf}^2 q_{ur}^2 P^{f}_{ur/\{1\}^{f}}\overline{P}^{f}_{ur/\{1\}^{f}} + 2q_u^2 q_{uf}^2 q_{ur}q_{ud}P^{f}_{ur}\\
&+ 2q_u^2 q_{uf}q_{ub}q_{ur}\Big[P^{f}_{ur/\{1\}^{b}}\Big(1 - P^{b}_{ur/\{1\}^{f}}\overline{P}^{b}_{ud}\Big)\\
&+ \overline{P}^{f}_{ur/\{1\}^{b}}P^{b}_{ur/\{1\}^{f}}\overline{P}^{b}_{ud}\Big] + 2q_u^2 q_{ub}q_{uf}q_{ud}P^{b}_{ur}\overline{P}^{b}_{ud/\{1\}^{f}}\\
&+ q_1^2 q_{ub}^2\Big[2P^{b}_{ur/\{1\}^{b}}\overline{P}^{b}_{ud/\{1\}^{b}}\Big(1 - P^{b}_{ur/\{1\}^{b}}\overline{P}^{b}_{ud/\{1\}^{b}}\Big)\Big].
\end{aligned} \tag{19}
$$

$$
\begin{aligned}
p^1_1 = \overline{q}_r p^0_1 + q_r\Big[&2q_u\overline{q}_u q_{uf}q_{ur}P^{f}_{ur}\overline{P}^{f}_{rd}\\
&+ 2q_u\overline{q}_u q_{ub}P^{b}_{ur}\overline{P}^{b}_{ud/\{r\}^{f}}\overline{P}^{f}_{rd/\{1\}^{b}}\\
&+ 2q_1^2 q_{uf}^2 q_{ud}q_{ur}P^{f}_{ur}\overline{P}^{f}_{rd/\{1\}^{f}}\\
&+ 2q_u^2 q_{uf}q_{ub}q_{ud}P^{b}_{ur}\overline{P}^{b}_{ud/\{1,r\}^{f}}\overline{P}^{f}_{rd/\{1\}^{f},\{1\}^{b}}\\
&+ q_u^2 q_{uf}^2 q_{ur}^2\Big(P^{f}_{ur/\{1\}^{f}}\overline{P}^{f}_{ur/\{1\}^{f}}\overline{P}^{f}_{rd} + (P^{f}_{ur/\{1\}^{f}})^2 P^{f}_{rd}\Big)
\end{aligned}
$$

$$
\begin{aligned}
&+ q_u^2 q_{ub}^2 \Big(2P^b_{ur/\{1\}^b} \overline{P}^b_{ud/\{r\},\{1\}} \overline{P}^f_{rd/\{2\}^b} \\
&\times (1 - P^b_{ur/\{1\}^b} \overline{P}^b_{ud/\{r\}^f,\{1\}^b}) \\
&+ (P^b_{ur/\{1\}^b} \overline{P}^b_{ud/\{r\}^f,\{1\}^b})^2 P^f_{rd/\{2\}^b} \Big) \\
&+ 2q_u^2 q_{ub} q_{uf} q_{ur} \Big(P^b_{ur/\{1\}^f} \overline{P}^b_{ud/\{r\}^f} \overline{P}^f_{ur/\{r\}^f,\{1\}^b} \overline{P}^f_{rd/\{1\}^b} \\
&+ (1 - P^b_{ur/\{1\}^f} \overline{P}^b_{ud/\{r\}^f}) P^f_{ur/\{1\}^b} \overline{P}^f_{rd/\{1\}^b} \\
&+ P^b_{ur/\{2\}^f} \overline{P}^b_{ud/\{r\}^f} P^f_{ur/\{1\}^b} P^f_{rd/\{1\}^b} \Big) \Big].
\end{aligned} \tag{20}
$$

$$
\begin{aligned}
p_2^0 = &\Big(q_u q_{uf} q_{ur} P^f_{ur/\{1\}^f} \Big)^2 + \Big(q_u q_{ub} P^b_{ur/\{1\}^b} \overline{P}^b_{ud/\{r\}^f,\{1\}^b} \Big)^2 \\
&+ 2q_1^2 q_{ub} q_{uf} q_{ur} P^b_{ur/\{1\}^f} \overline{P}^b_{ud} P^f_{ur/\{1\}^b}.
\end{aligned} \tag{21}
$$

$$
\begin{aligned}
p_2^1 = \overline{q}_r p_2^0 + q_r \Big[&\Big(q_u q_{uf} q_{ur} P^f_{ur/\{1\}^f} \Big)^2 \overline{P}^f_{rd} \\
&+ \Big(q_u q_{ub} P^b_{ur/\{1\}^b} \overline{P}^b_{ud/\{r\}^f,\{1\}^b} \Big)^2 \overline{P}^f_{rd/\{2\}^b} \\
&+ 2q_1^2 q_{ub} q_{uf} q_{ur} P^b_{ur/\{1\}^f} \overline{P}^b_{ud} P^f_{ur/\{1\}^b} \overline{P}^f_{rd/\{1\}^b} \Big].
\end{aligned} \tag{22}
$$

REFERENCES

[1] G. Kramer, I. Marić, and R. D. Yates, "Cooperative communications," *Found. Trends Netw.*, vol. 1, no. 3, pp. 271–425, Aug. 2006.

[2] A. K. Sadek, K. J. R. Liu, and A. Ephremides, "Cognitive multiple access via cooperation: Protocol design and performance analysis," *IEEE Transactions on Information Theory*, vol. 53, no. 10, pp. 3677–3696, Oct. 2007.

[3] N. Pappas, A. Ephremides, and A. Traganitis, "Relay-assisted multiple access with multi-packet reception capability and simultaneous transmission and reception," in *IEEE Information Theory Workshop*, Oct. 2011, pp. 578–582.

[4] N. Pappas, M. Kountouris, A. Ephremides, and A. Traganitis, "Relay-assisted multiple access with full-duplex multi-packet reception," *IEEE Transactions on Wireless Communications*, vol. 14, no. 7, pp. 3544–3558, July 2015.

[5] G. Papadimitriou, N. Pappas, A. Traganitis, and V. Angelakis, "Network-level performance evaluation of a two-relay cooperative random access wireless system," *Computer Networks*, vol. 88, pp. 187–201, Sept. 2015.

[6] B. Xie, Z. Zhang, and R. Q. Hu, "Performance study on relay-assisted millimeter wave cellular networks," in *IEEE 83rd Vehicular Technology Conference (VTC Spring)*, May 2016, pp. 1–5.

[7] S. Biswas, S. Vuppala, J. Xue, and T. Ratnarajah, "On the performance of relay aided millimeter wave networks," *IEEE Journal of Selected Topics in Signal Processing*, vol. 10, no. 3, pp. 576–588, Apr. 2016.

[8] J. W. Sungoh Kwon, "Relay selection for mmwave communications," in *the 28th Annual IEEE International Symposium on Personal, Indoor and Mobile Radio Communications (IEEE PIMRC)*, Oct. 2017, pp. 1–5.

[9] Y. Xu, H. Shokri-Ghadikolaei, and C. Fischione, "Distributed association and relaying with fairness in millimeter wave networks," *IEEE Transactions on Wireless Communications*, vol. 15, no. 12, pp. 7955–7970, Dec. 2016.

[10] N. Wei, X. Lin, and Z. Zhang, "Optimal relay probing in millimeter-wave cellular systems with device-to-device relaying," *IEEE Transactions on Vehicular Technology*, vol. 65, no. 12, pp. 10 218–10 222, Dec. 2016.

[11] S. Wu, R. Atat, N. Mastronarde, and L. Liu, "Coverage analysis of d2d relay-assisted millimeter-wave cellular networks," in *IEEE Wireless Communications and Networking Conference (WCNC)*, Mar. 2017, pp. 1–6.

[12] R. Congiu, H. Shokri-Ghadikolaei, C. Fischione, and F. Santucci, "On the relay-fallback tradeoff in millimeter wave wireless system," in *IEEE Conference on Computer Communications Workshops (INFOCOM WKSHPS)*, Apr. 2016, pp. 622–627.

[13] S. Sun, T. S. Rappaport, R. W. Heath, A. Nix, and S. Rangan, "Mimo for millimeter-wave wireless communications: beamforming, spatial multiplexing, or both?" *IEEE Communications Magazine*, vol. 52, no. 12, pp. 110–121, Dec. 2014.

[14] T. Bai and R. W. Heath, "Coverage and rate analysis for millimeter-wave cellular networks," *IEEE Transactions on Wireless Communications*, vol. 14, no. 2, pp. 1100–1114, Feb. 2015.

[15] R. M. Loynes, "The stability of a queue with non-independent inter-arrival and service times," *Mathematical Proceedings of the Cambridge Philosophical Society*, vol. 58, no. 3, pp. 497–520, 1962.

[16] F. Gebali, *Analysis of Computer and Communication Networks*. New York, NY, USA: Springer-Verlag, 2010.

[17] 3GPP, "Study on channel model for frequencies from 0.5 to 100 GHz (release 14), 3gpp tr 38.901 v14.2.0," Tech. Rep., Sept. 2017.